# Accepted Manuscript


Neoarchean crustal growth and Paleoproterozoic reworking in the Borborema Province, NE Brazil: Insights from geochemical and isotopic data of TTG and metagranitic rocks of the Alto Moxotó Terrane

Lauro Cézar Montefalco de Lira Santos, Elton Luiz Dantas, Peter A. Cawood, Edilton José dos Santos, Reinhardt A. Fuck

PII: S0895-9811(16)30247-4

DOI: 10.1016/j.jsames.2017.08.013

Reference: SAMES 1754

To appear in: *Journal of South American Earth Sciences*

Received Date: 5 November 2016

Revised Date: 23 July 2017

Accepted Date: 16 August 2017

Please cite this article as: Montefalco de Lira Santos, Lauro.Cé., Dantas, E.L., Cawood, P.A., José dos Santos, E., Fuck, R.A., Neoarchean crustal growth and Paleoproterozoic reworking in the Borborema Province, NE Brazil: Insights from geochemical and isotopic data of TTG and metagranitic rocks of the Alto Moxotó Terrane, *Journal of South American Earth Sciences* (2017), doi: 10.1016/j.jsames.2017.08.013.

# Proposed tectonic settings

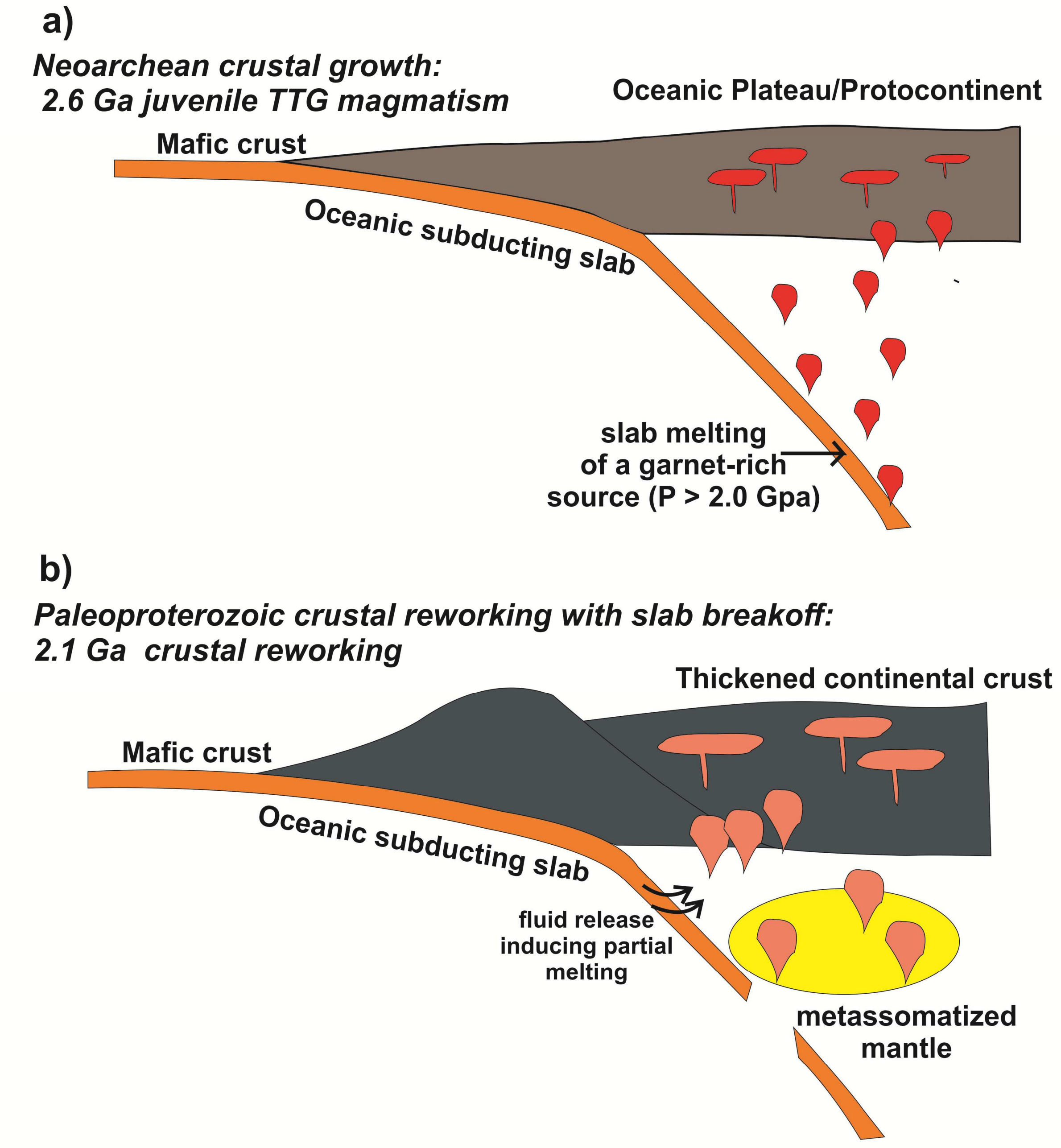

# Neoarchean crustal growth and Paleoproterozoic reworking in the Borborema Province, NE Brazil: Insights from geochemical and isotopic data of TTG and metagranitic rocks of the Alto Moxotó Terrane

Lauro Cézar Montefalco de Lira Santos[1,2,*]; Elton Luiz Dantas[1]; Peter A. Cawood[3,4]; Edilton José dos Santos[5]; Reinhardt A. Fuck[1];

[1]Instituto de Geociências, Universidade de Brasília, Brazil; [2]Unidade Acadêmica de Mineração e Geologia, Universidade Federal de Campina Grande, Brazil; [3]School of Earth, Atmosphere and Environment, Monash University, Victoria 3800, Australia; [4]Department of Earth Sciences, University of St Andrews, St Andrews KY16 9AL, UK; [5]Serviço Geológico do Brasil - CPRM, Brazil.; *Corresponding author. E-mail: lauromontefalco@gmail.com

Highlights

> First record of Archean Continental Crust in Central Subprovince of the Borborema Province;

> Geochemical and isotopic data reveals a complex accretionary history for the Alto Moxotó Terrane;

> Our data provide evidence for new Neoarchean crustal growth and Paleoproterozoic reworking in central Western Gondwana.


## ABSTRACT

Pre-Brasiliano rocks in the Borborema Province (NE Brazil) are concentrated in basement blocks, such as the Alto Moxotó Terrane. Petrographic, geochemical, and U-Pb and Sm-Nd isotopic data from two basement metagranitic suites within the terrane provide evidence for Neoarchean (2.6 Ga) and Paleoproterozoic (2.1 Ga) subduction-related events. The Riacho das Lajes Suite is made of medium to coarse-grained hornblende and biotite-bearing metatonalites and metamonzogranites. Whole-rock geochemical data indicate that these rocks represent calcic, magnesian and meta- to peraluminous magmas, and have unequivocal affinities with high-Al low-REE tonalite-trondhjemite-granodiorites (TTG). Zircon U-Pb data from two samples of this suite indicate that they were emplaced at 2.6 Ga, which is the first discovered Archean crust in the central portion of the province. The suite has Neoarchean depleted mantle model ages ($T_{DM}$) and slightly negative to positive εNd(t), indicating slight crustal contamination. The overall geochemical and isotopic data indicate a Neoarchean intraoceanic setting for genesis of the Riacho das Lajes magma via melting of basaltic oceanic crust submitted to high-pressure eclogite facies conditions. On the other hand, the Floresta Suite comprise metaigneous rocks, which are mostly tonalitic and granodioritic in composition. Geochemical data indicate that this suite shares similarities with calcic to calc-alkalic magmas with magnesian and metaluminous to slightly peraluminous characteristics. Other geochemical features include anomolous Ni, V and Cr contents, as well as high large-ion litophile elements (LILE) values. The suite yields U-Pb zircon ages of approximately 2.1 Ga, Archean to Paleoproterozoic $T_{DM}$ ages, and negative to positive εNd(t) values, suggesting both new crust formation and reworking of Archean crust, in addition to mantle metasomatism, reflecting mixed sources. The most likely tectonic setting for the Floresta Suite magmas involved crustal thickening by terrane accretion, coeval to slab break off. Our results provide new insights on proto-Western Gondwana crustal evolution.

Keywords: Crustal growth; continental reworking; Neoarchean TTG; Western Gondwana; Borborema Province.

## 1. Introduction

The recognition of major petrogenetic controls on formation and recycling of preexisting crust in yunger orogenic provinces provide important insights on major cratonic connections. For instance, it has been suggested that some reworked basement inliers/terranes may eventually represent missing crustal puzzles of continents or supercontinents, such as Atlantica and Nuna/Columbia (Reddy and Evans, 2009; Rogers and Santosh, 2009; Neves, 2011).

The preserved record for the generation of continental crust is episodic, its formation being related to juvenile magmatism in subduction-related (Niu and O´Hara 2009; Cawood et al., 2013) or mantle plume (Condie, 1998) settings. Conversely, recycling of continental crust back to the mantle may have been active since the Paleoarchean, and coeval with crustal growth events (Cavosie et al., 2006; Arndt, 2013).

In the Archean, high heat production and accretion rates favored the generation of specific petrogenetic associations, such as komatiites in granite-greenstone terranes and voluminous tonalite-trondhjemite-granodiorite (TTG) magmas (Martin et al., 2005). In contrast, during the Archean-Proterozoic transition, changes in geodynamic processes resulted in a decrease of TTG production, followed by a strong increase in the generation of more potassic and less sodic granitoids (Shirey and Hanson 1984, Smithies and Champion, 2000; Laurent et al., 2014). In several cratonic blocks, these compositional changes are recorded in juvenile plutonic and volcanic suites related to a major 2.7-2.5 Ga crustal growth event, which is considered to be one of the most important periods of continental crust generation in Earth's history (Condie, 2000; Hawkesworth et al., 2010; Condie and Kröner 2013; Wan et al., 2014).

Experimental studies indicate that unlike normal calc-alkaline magmas, TTG-like geochemical signature results from a moderate degree of partial melting of hydrated basaltic (low-K) crust at pressures high enough to stabilize garnet±amphibole paragenesis (Rapp and Watson 1995; Martin et al., 2005). The classic tectonic scenario for TTG genesis is usually attributed to subduction-related settings, in which partial melting of subducted oceanic crust (meta-basalts) under high pressure conditions is induced by elevated Archean geothermal gradients (Defant and Drummon, 1990; Rapp et al., 2003; Halla et al., 2009; Laurent et al., 2014). Other possible scenarios include the development of a thick oceanic plateau due to mantle plume over oceanic crust (Smithies and Champion 2000; Zegers and van Keken 2001; Condie, 2005) and the delamination of an over-thickened mafic crust (Johnson et al., 2013).

Continental magmatic arcs are widespread in the Paleoproterozoic (Rogers and Santosh, 2003; Zhao et al., 2004). They are responsible for the production of a large compositional range of volcanic and plutonic rocks (Tatsumi and Eggins, 1995). In such settings, the most accepted mechanism of melt generation involves progressive releasing of aqueous fluids or silicate melts from the subducting slab. This gradual process induces partial melting of the overlying mantle wedge by reducing its solidus temperature (van Keken et al., 2002; Kelley et al., 2010), leading to the formation of magmas with unique arc geochemistry. It has been argued that the generation of these arc magmas contributes directly to formation of new crust and/or reworking of early formed continental margins (Rudnick, 1995; Hollister and Andronicos, 2006).

Recently, several ancient basement terranes/domains and granitoids representing variable sources has been documented in the Neoproterozoic Brasiliano-Pan African belts revealing complex pre-Western Gondwana scenarios (e.g. Neves et al., 2015; Santos et al., 2015). However, petrological and geochronological studies are still scarce, mostly due the strong reworking during Neoproterozoic orogenesis.

In this work, we present whole-rock geochemical and Sm-Nd isotopic data and U-Pb zircon age determinations of the basement Riacho das Lajes and Floresta suites of the Alto Moxotó Terrane, central portion of the Borborema Province (BP). Our main goals are to: (1) identify the nature of their sources and tectonic setting; (2) determine the timing of intrusion and associated crust-related processes (crustal growth vs. reworking); and (3) constrain geodynamic processes through integration of data from across the Borborema Province and other domains of Western Gondwana.

## 2. Regional Geology

### 2.1 Borborema Province

The Borborema Province is the largely exposed, northeastern portion of the Precambrian basement of the South American Platform (Almeida et al., 1981). It is located in the central part of Western Gondwana and is part of a large and complex orogenic system that extends through the Pan-African fold-belts between Togo to the north and Cameroon to the east in Central Africa (Fig. 1a; Brito Neves 1975; Trompette 1994; de Wit et al., 2008; Van Schmus et al., 2008, 2011).

The geologic configuration of the BP includes basement complexes with Paleoproterozoic ages as well as local exposures of Archean nuclei, in which constituent orthogneisses and migmatites have been inferred to have formed by subduction-related and minor within-plate-related processes (Brito Neves et al., 2000; Santos et al., 2000; Fetter et al., 2003; Van Schmus et al., 2008; Martins et al., 2009; Brito Neves, 2011; Neves et al., 2015; Santos et al., 2015a). In addition, the province includes early to late Neoproterozoic supracrustal fold belts and magmatic arcs containing widespread granitic magmatism related to Brasiliano orogenesis (Santos and Medeiros, 1999;

Kozuch, 2003; Santos et al., 2010; Caxito et al., 2014a, b; Ganade de Araújo et al., 2014a,b,c).

The province is transected by a complex network of E-W and NE-SW crustal-scale strike-slip shear zones with mylonites up to several kilometers across (Vauchez et al., 1995; Archanjo et al., 2008). It is divided into the Northern, Central and Southern subprovinces (Fig. 1b; Van Schmus et al., 1995, 2008; Brito Neves et al., 2000). Available isotopic and structural data have led to the suggestion that the province was subjected to a polycyclic tectonic evolution involving episodes of accretion of tectono-stratigraphic terranes during the Neoproterozoic (Santos 1996; Santos and Medeiros, 1999; Santos et al., 2010; Brito Neves et al., 2005, 2014; Santos et al., 2015b). However, an intracontinental orogen hypothesis has also been invoked for the evolution of the BP (Neves, 2015). For this reason, we follow the original terrane definition of Coney et al., (1980), which is exclusively descriptive.

2.1.1. Central Subprovince

The Central Subprovince occupies the central portion of the BP and is bounded by the regional Patos and Pernambuco lineaments to the north and south, respectively. It was affected by the Cariris Velhos orogenic event at ca. 1.0 Ga, followed by the Brasiliano orogeny at ca. 0.6 Ga (Van Schmus et al., 1995; Santos, 1996; Santos and Medeiros, 1999; Santos et al., 2010; Brito Neves et al., 2014).

From west to east five terranes are recognized in the Central Subprovince: São José do Caiano (SJC), Piancó-Alto Brígida (PABT), Alto Pajeú (APT), Alto Moxotó (AMT), and Rio Capibaribe (RCT) (Fig. 1c). NE-SW trending strike-slip shear zones cut across these crustal blocks. Neoproterozoic felsic and mafic plutons occur throughout the Subprovince along with Paleo- and Neoproterozoic supracrustal fold belts (Santos and Medeiros, 1999). Early Paleoproterozoic units are concentrated in the Alto Moxotó Terrane and in some areas of the Rio Capibaribe Terrane, whereas Archean rocks have not previously been described from the Central Subprovince (see Neves et al., 2015 and Santos et al., 2015a for details).

#### 2.1.1.1. The Alto Moxotó Terrane

The Alto Moxotó Terrane (AMT) is a high-grade metamorphic block composed of metaplutonic suites, including metagranites, orthogneisses, migmatites and mafic-ultramafic rocks in addition to supracrustal sequences that are interpreted by some authors as Paleoproterozoic in age (Rodrigues and Brito Neves 2008; Santos et al., 2004, 2012, 2013). Up to now, there is no consensus on the location of the boundary of this terrane with the Alto Pajeú Terrane. The Serra de Jabitacá and Afogados da Ingazeira shear zones are the main candidates for this boundary (Santos and Medeiros 1999; Rodrigues and Brito Neves, 2008). The southern limit of the AMT is represented by the strike-slip Pernambuco lineament and the Congo Cruzeiro do Nordeste shear zone (Brito Neves et al., 2013).

A long-lived Paleoproterozoic tectono-magmatic evolution for the AMT, divided into three main tectonic pulses, has been proposed by Santos et al. (2015a). The first tectonic event was responsible for the emplacement of intermediate metaplutonic rocks with a magmatic arc-related signature, which are Siderian in age with both juvenile and crustal characteristics. The second event is represented by granodioritic to tonalitic gneisses and mafic-ultramafic magmatism, also in a subduction-related setting, but with a stronger crustal signature at 2.1-2.0 Ga. This event was responsible for multiple sheet-like intrusions that are widespread throughout the terrane. The final Paleoproterozoic igneous activity is characterized by within-plate bimodal magmatism dated at 1.6 Ga (Santos et al., 2015a). Cambrian granites occur along the margins of the Alto Moxotó Terrane.

[Fig. 1 near here]

## 3. Local Geology

The study area is located in the SW portion of the Alto Moxotó Terrane, close to Floresta, and comprises a series of metaplutonic and supracrustal sequences (Fig. 2). The Riacho das Lajes Suite is separated by SSE-verging contractional shear zones from the Riacho do Navio Suite (highly deformed augen-gneisses) to the north and the Sertânia Complex (garnet paragneisses and migmatites) to the south. The Floresta Suite forms a batholith along the south rim of the terrane, in tectonic contact with the southern Subprovince along the Pernambuco Lineament. Contact relationship with the supracrustal rocks of the Sertânia Complex is poorly understood due to the strong 0.6 Ga Brasiliano deformation that affected the region.

[Fig. 2 near here]

### *3.1. Riacho das Lajes Suite*

This suite was previously described as a series of white metagranitoids and orthogneisses with trondhjemitic affinity (Santos, 1995). It is formed by leucocratic rocks that are elongated E-W and NE-SW due to Neoproterozoic Brasiliano deformation. The suite occupies the central part of the study area, where two main facies were identified: i) slightly deformed granitoids (Fig. 3a); and ii) strongly foliated members forming orthogneisses (Fig. 3b) that show mafic-felsic streaky compositional banding and scarce occurrences of E-W oriented, 30-50 cm long mafic enclaves. Additionally, partially migmatized facies occur locally and are characterized by metatexites with well-preserved paleosome, but local bands of leucosomes are present and occur parallel to the regional foliation forming stromatic fabrics (Fig. 3c). Discordant quartz-feldspar veins also occur, which is a typical feature of vein-structured migmatites.

Petrographic analysis indicates that these rocks represent holo-leucocratic, leucocratic and mesocratic protoliths, ranging from tonalite to granodiorite in composition, but quartz monzodioritic and monzogranitic variations are also present (Fig. 4). They are medium to coarse-grained (1.0 to 5.0 mm in diameter). The less deformed samples are characterized by hypidiomorphic to allotriomorphic granular textures, in contrast with dominant granoblastic polygonal texture in the most deformed members. The groundmass mineralogy of Riacho das Lajes granitoids includes plagioclase (oligoclase-andesine) (40-42%) and quartz (35-38%) (Fig. 5a). Plagioclase crystals form hypidiomorphic prismatic grains that can preserve relicts of myrmekitic intergrowths with irregular quartz crystals. In addition, the former is locally zoned, indicating abrupt changes in magma composition, whereas the quartz grains are idioblastic, hypidioblastic or xenoblastic. Polygonal shapes are common in the most deformed samples, suggesting intense recrystallization.

Quartz grains also occur as static rotated grains or exhibit ribbon-like structures with frequent undulose extinction, which reflects intense post-crystallization deformation (Fig. 5b). In some samples, the local deformation is also characterized by grain orientations alternating millimeter-size felsic and mafic minerals (mainly biotite), thus indicating metamorphic segregation. K-feldspar grains (~10%) may exhibit perthitic intergrowth but are rare. Hypidioblastic microcline grains exhibit crosshatch crystal twinning, but irregular orthoclase aggregates are also common. Dark to reddish brown biotite (5-15%) (Fig. 5c) and greenish hornblende (5-10%) are widespread in all samples and represent the main ferromagnesian phases. Minor clinopyroxene crystals are also present (2-3%). The accessory minerals include hypidioblastic titanite (1-2%), xenoblastic allanite (1-2%), idioblastic apatite (1%) and hypidioblasic zircon (1%). Magnetite (2-3%) is the main opaque mineral, and the occurrence of hypidioblastic chlorite crystals (1%) represents the main secondary phase, which we interpret as the result of biotite alteration.

### 3.2. Floresta Suite

This suite corresponds to part of the Floresta Complex defined by Lima et al. (1985). Several petrographic types were distinguished by Santos (1995), including amphibolites, metatonalites, metadiorites and metagranodiorites. According to these authors, the Floresta Complex corresponds to the regional basement of the entire Alto Moxotó Terrane. Recent work by Santos et al. (2013, 2015a) as well as the present study reveals that the Floresta Complex consists of a series of metaplutonic suites on the basis of field, petrographic and isotopic data. In this paper, we describe a new unit of the Floresta Complex, termed the Floresta Suite.

The Floresta Suite is an approximately 30 km long, E-W elongated batholith with interleaving mafic-ultramafic rocks (metagabbros, metapyroxenites and metaperidotites) refered to as the Malhada Vermelha Suite (Santos, 1995). Its shape is controlled by the Brasiliano strike-slip Pernambuco lineament along the south rim of the body. The suite shows strong structural zonation, with less deformed members in its central part (Figs. 3d and 3e) and progressively more intensively foliated rocks towards its margins, forming orthogneissic facies with mafic-felsic compositional banding (Fig. 3f), as well as developing mylonitic to ultra-mylonitic fabric. Local migmatization is also present and is characterized by discrete stromatic and folded structures. The main rock associations comprise biotite-bearing and hornblende-bearing metaplutonic members, including granodioritic, dioritic, quartz-dioritic, tonalitic and monzogranitic compositions (Fig. 4).

Fine-, medium- and coarse-grained (0.25 to 5 mm in diameter) irregular groundmass is mostly dominated by granoblastic and less nematoblastic texture (Figs. 5d, 5e). Granoblastic polygonal fabric is very common in the most deformed samples and is characterized by equidimensional grains forming local triple junctions. Subdioblastic and xenoblastic textures are present in strongly foliated samples. Mineralogically, the suite consists of a subdiomorphic aggregate mass of quartz (35-40%), plagioclase (35-40%) and K-feldspar (10-15%), with hornblende and biotite as the main mafic phases.

Quartz grains are recrystallized with sutured boundaries exhibiting undulose extinction, whereas plagioclase crystals (oligoclase to andesine) are primarily hypidioblastic to xenoblastic with local mymerkitic intergrowth relicts. Idioblastic microcline is the most common potassic feldspar, but orthoclase grains are also present, exhibiting patch and vein type perthites, as well as quartz and biotite inclusions.

The main mafic phases are represented by large deformed greenish hornblende crystals (10-15%, Fig. 5f) and bent flakes of dark brown biotite (5-7%), which can also replace hornblende crystals. Xenoblastic clinopyroxene clusters are present in lesser amounts (2%). Titanite (1-2%) is the most common accessory phase in these rocks, indicating early crystallization in the protolith progenitor magma. Well-formed apatite and zircon crystals are other common accessories, representing less than 2% of the rock composition. Opaque minerals are represented by small magnetite crystals (less than 1%). Chlorite crystals are rare and result from biotite alteration (less than 1%).

[Fig. 3 near here]

[Fig. 4 near here]

[Fig. 5 near here]

## 3. Analytical Procedures

Fresh representative rock samples were analyzed for major and trace elements at Acme Analytical Laboratories Ltd. (Canada). Major elements were determined by inductively coupled plasma-emission spectrometry, with a detection limit of 0.01% and precision of ± 0.1%. Trace elements were analyzed by inductively coupled plasma-mass spectrometry (ICP-MS), with detection limits between 0.01 and 0.5 ppm and precision of ± 5%. Geochemical diagrams were generated using Igpet 06 software, GCDkit, Petrograph and Excel sheets.

Four samples, two for each studied unit, were selected for zircon U-Pb age dating at the Geochronology Laboratory of Universidade de Brasilia, Brazil. The samples were initially crushed and sieved, and then the heavy minerals were separated using conventional gravimetric and magnetic methods. Zircon grains were then handpicked using a binocular microscope and mounted on epoxy resin for Laser Ablation Inductively Coupled Plasma Mass Spectrometry (LA-MC-ICP-MS) isotope ratio acquisition. Data reduction was performed following Bühn et al. (2009) and Matteini et al. (2009). Isotopic analyses were performed on a Thermo Finnigan Neptune Multi-collector ICPMS equipped with a secondary electron multiplier-ion counter at the Geochronology Lab of the University of Brasilia. Cathodoluminescence and back-scattered images were used to investigate the internal structure of the zircon crystals prior to each analysis. Only coherent interval analyses were chosen to avoid signal mixed ages. Normalization was performed with internal GJ standard zircon (608.5 ± 1.5 Ma; Jackson et al., 2004), and the age calculations were performed using in-house developed Excel spreadsheets.

For the Sm-Nd data, an 24 samples from both studied suites were analyzed, following the method described by Gióia and Pimentel (2000). Whole rock powders (ca. 50 mg) were mixed with a $^{149}$Sm-$^{150}$Nd spike solution and dissolved in Savillex capsules. Extraction of Sm and Nd from whole-rock samples followed conventional cation exchange techniques, using Teflon columns containing LN-Spec resin (HDEHP – diethylhexyl phosphoric acid supported on PTFE powder). Sm and Nd samples were loaded on double-filament of Re evaporation assemblies, and the isotopic measurements were also performed on a multi-collector Finnigan MAT 262 mass spectrometer in static mode at the University of Brasilia. Uncertainties in the Sm/Nd and $^{143}$Nd/$^{144}$Nd ratios are better than ± 0.4% (1 σ) and ± 0.005% (1 σ), respectively, based on repeated analyses using the international rock standards BHVO-1 and BCR-1. $^{143}$Nd/$^{144}$Nd ratios were normalized to a $^{146}Nd/^{144}Nd$ of 0.7219, and the decay constant used was 6.54 x $10^{-12}$. Depleted mantle model age values were calculated using the DePaolo (1981) model.

## 4. Results

### 4.1. Geochemistry

#### 4.1.1 Riacho das Lajes Suite

Eleven samples of metagranitoid and orthogneiss from this suite were selected for geochemical analysis, and the results are listed in Table 1. On the ternary diagram of normative feldspar composition (O´Connor, 1965) the samples show a relatively narrow compositional range, corresponding mostly to granodiorites and tonalites, but granite and quartz monzonite compositions are also present (Fig. 6a).

$SiO_2$ values for the Riacho das Lajes Suite range from 69.8 to 76.4 wt.%, $Na_2O$ from 3.98 to 5.07 wt.%, and $K_2O$ from 0.83 to 4.23 wt.%. On the alkali-lime index vs. silica diagram the samples are calcic (CaO ranging from 2.54 to 3.39 wt.%, Fig. 6b). The samples are mostly magnesian, with minor iron enrichment (MgO and FeO values ranging from 0.15 to 1.02 wt.% and 0.9 to 3.3 wt.%, respectively), and are chemically similar to Cordilleran granites (Fig. 6c). $Al_2O$ values range from 13.8 to 16.95 wt.% and plot in the peraluminous and metaluminous fields of the A/NK vs. A/CNK diagram (Fig. 6d). On the K-Na-Ca diagram, the samples show a small sodic tendency but also slight K enrichment, and they do not follow the trondhjemitic or the calc-alkaline trends (Fig. 6e).

On primitive-mantle normalized multi-element diagram (spider diagram) the Riacho das Lajes Suite displays a uniform pattern (Fig. 7a) characterized by moderate to high contents of large ion lithophile elements (LILE) and high field strength elements (HFSE). Strong Nb, P and Ti negative anomalies are observed, in addition to discrete to moderate depletions of Ce, Sm and Lu in most samples. Pb and Zr mark positive peaks. A steep rare earth elements pattern in reference to chondrite is clearly observed in the studied samples (Fig. 7b). This behavior is characterized by strong enrichment of light rare earth elements (LREE) with respect to most heavy rare earth elements (HREE)

($[La/Yb]_N$ = 55.68 - 175.85). The samples also display a pronounced positive Eu peak (Eu/Eu* varying between 1.15 and 2.10).

[Table 1 near here]

4.1.2. Floresta Suite

Seventeen samples of the Floresta Suite were selected for whole-rock geochemical determination, and the results are given in Table 2. Chemically, they correspond primarily to tonalites, granites and granodiorites on the ternary diagram of normative feldspar composition (Fig. 6a). They are characterized by $SiO_2$, ranging from 52.5 to 76.7 wt.%, whilst $Na_2O$ values are rather homogeneous and range from 2.52 to 4.22 wt.%. CaO and $K_2O$ contents are variable, ranging from 1.15 to 8.83 wt.% and 0.71 to 5.49 wt.%, respectively. On the alkali-lime index vs. silica diagram, the samples show a calcic to calc-alkalic trend (Fig. 6b). On the FeOt/(FeO + MgO) diagram (Frost et al., 2001), they plot mainly in the magnesian field, sharing chemical similarities with classic Cordilleran type-granites (MgO ranging from 0.23 to 5.22 wt.% and FeO ranging from 1.45 to 9.6 wt.%, Fig. 6c). The $Al_2O_3$ values range from 13.15 to 20.8 wt.%, and on the A/NK vs. A/CNK diagram, using the alumina saturation index, these rocks can be characterized as metaluminous to slightly peraluminous (Fig. 6d), whereas on the K-Na-Ca diagram, although somewhat dispersed, they follow the calc-alkaline trend (Fig. 6e). The primitive mantle-normalized spider diagram for the Floresta Suite displays moderate to high values of large ion lithophile elements (LILE). The high field strength elements (HFSE) behavior is marked by negative anomalies of Nb; P and Ti also show important negative peaks (Fig. 7c). In terms of rare earth elements (REE) content, the samples from this suite exhibit moderate to high fractionation of LREE compared to HREE ($[La/Yb]_N$ = 7.07 - 108.70), and negative to positive Eu anomalies, which are generally induced by plagioclase accumulation in the melt (Eu/Eu* varying between 0.38 and 2.09) (Fig. 7d).

[Table 2 near here]

[Fig. 6 near here]

[Fig. 7 near here]

4.2. U-Pb Geochronology

U-Pb zircon data for the Riacho das Lajes and Floresta suites are presented in tables 3, 4, 5 and 6. Cathodoluminescence images were used as a guide for spot selection of representative zircon grains and are shown in Fig. 8.

[Table 3 near here]

[Table 4 near here]

[Table 5 near here]

[Table 6 near here]

[Fig. 8 near here]

4.2.1. Riacho das Lajes Suite

Sample FL-56 is a white to light-gray, coarse-grained metatonalite. This sample was collected 10 km east of Airi (coordinates: 8º30'12"S and 38º5'30"W). The majority of the dated zircon grains are idiomorphic and have well-developed oscillatory zoning, with dimensions ranging from 120 to 240 µm. Most of the grains have a discrete metamorphic overgrowth due to later thermal events. However, most of the grains present Th/U ratios varying from 0.10 to 0.46, which attests to a magmatic origin. The analyses of zircon grains from this sample result in a Discordia line with an upper intercept of 2625 ± 14 Ma (MSWD = 3.9), which is interpreted as the crystallization age of the tonalitic protolith (Fig. 9).

The second dated sample (FL-105) corresponds to a discretely banded granodiorite orthogneiss, collected near Airi. Zircon crystals from this sample are euhedral, subhedral and anhedral. The geographical coordinates are 8º29'16"S and 38º12'24"W. Some exhibit oscillatory zoning and around 100 µm on average. The majority of the analyzed zircon grains present Th/U ratios ranging from 0.12 to 0.4, which correspond to igneous crystals, but in various grains pronounced metamorphic overgrowth can be observed, which is probably due to later thermal events that affected the region. The analyzed grains resulted in a Discordia line that yields an upper intercept age of 2643 ± 18 Ma (MSWD = 1.9), which is interpreted as the crystallization age of the granodiorite protolith (Fig. 10). The ages of 560 ± 36 Ma and 645 ± 85 Ma observed in the lower intercepts of samples FL-56 and FL-105, respectively, are interpreted as the result of Pb loss during the Brasiliano orogeny that strongly affected most of the Borborema Province (Brito Neves, 2014).

[Fig. 9 near here]

[Fig. 10 near here]

4.2.2. Floresta Suite

Sample FL-65 corresponds to a dark gray inequigranular, biotite-bearing, medium-grade metadiorite with pronounced metamorphic foliation, collected near the Barragem locality (coordinates 8º34'44"S and 38º22'33W). The selected hypidiomorphic to idiomorphic zircon grains are colorless to dark grey and display some cracks in inner domains. They range from 100 to 140 µm and their Th/U ratios range from 0.190 to 0.426, indicating an igneous origin. The Concordia diagram for the analyzed zircon grains yields an upper intercept age of 2103.8 ± 9.3 Ma (MSWD = 1.8), which is interpreted as the protolith crystallization age (Fig. 11).

Sample FL-60 is a pale gray inequigranular medium to coarse-grained metatonalite. This sample was collected in the central part of the Floresta Suite (coordinates 8º35'10"S and 38º26'00"W). Zircon grains from this sample are heterogeneous, subhedral, euhedral and anhedral and are 100 to 119 µm long. They have well-developed igneous oscillatory zoning surrounded by discrete metamorphic overgrowth. Th/U ratios range from 0.121 to 0.849. The Concordia diagram for this rock has a MSWD of 1.4, and the analyzed grains exhibit an upper intercept age of 2.098 ± 18 Ma (MSWD = 1.4), which is interpreted as the age of crystallization of the protolith (Fig. 12). FL-65 and FL-60 samples yield lower intercept ages of 492 ± 46 Ma and 457 ± 57 Ma, respectively, which are interpreted as the result of Pb loss related to later thermal effects.

[Fig. 11 near here]

[Fig. 12 near here]

4.4.3. Sm-Nd Isotopes

Sm-Nd isotope analyses were performed on seven representative samples of the Riacho das Lajes Suite and seventeen samples of the Floresta Suite. The corresponding isotopic compositions and isotopic ratios are presented in Table 7. Figure 13 shows the geographic distribution of the collected samples and the results, including those of the U-Pb data. The obtained εNd (t) values were calculated using the 2.625 and 2.098 Ga crystallization ages obtained for the Riacho das Lajes and Floresta suites, respectively (Fig. 14). The samples from the Riacho das Lajes suite yielded Meso- to Neoarchean Nd depleted mantle ($T_{DM}$) model ages ranging from 2.76 to 2.93 Ga and a narrow range of slightly negative and positive εNd (t) values (-2.35 to +0.36). The samples from the Floresta Suite present heterogeneous Archean to Paleoproterozoic $T_{DM}$ model ages (3.19 to 2.23 Ga). These data indicate the involvement of old crust in the genesis of these rocks. The εNd (t) values range from -12.03 to +4.47.

[Table 7 near here]

[Fig. 13 around here]

[Fig. 14 around here]

## 5. Discussion

### 5.1. Magma sources and tectonic setting

#### *5.1.1. Riacho das Lajes Suite*

Studied samples from the Riacho das Lajes Suite represent silicic, calcic, magnesian and slightly peraluminous magmas emplaced during the Neoarchean (ca. 2.6 Ga). The primitive mantle-normalized spider diagram shows strong depletions of Nb, Ta and Ti, which can be interpreted as the effect of rutile, sphene or Ti-bearing amphibole as residual phases in the source region (Foley et al., 2000; Klemme et al., 2006). Such negative anomalies in spider diagrams are very distinctive of subduction-related settings (Pearce, 1982). The chondrite-normalized REE diagram is characterized by the enrichment of light REE relative to heavy REE and exhibits positive Eu anomalies. Due to its high partition coefficient (Kd), garnet is usually invoked as the main residual phase. This mineral concentrates most of HREE, thereby generating magmas with very low concentrations of Er, Lu, Tm, Y and Yb, whereas Eu is easily accommodated in the plagioclase structure, and its high content suggests the enrichment of this phase in the melt.

General petrographic and geochemical data indicate that the Riacho das Lajes Suite samples have similar characteristics to classic Archean TTG or high-silica adakites. These include the i) dominant tonalite and granodiorite members, ii) high $SiO_2$ (> 70% wt.%) and Na2O (> 4 wt.%), iii) low MgO (<1 wt.%) and FeO (< 3 wt.%), iv) low $K_2O/Na_2O$ ratios (<0.4), and v) strongly fractionated REE pattern (Martin et al., 2005; Smithies and Champion, 2000; Condie, 2005; Castillo et al., 2006). However, they also display relatively high $K_2O$ contents (> 2 wt.%) compared to classic Archean TTGs. This fact can be explained by the greater extent of fractional crystallization or re-melting processes, which is fairly common in granitoid rocks related to the Neoarchean-Paleoproterozoic transition (Sylvester 1994; Moyen et al., 2003; Martin et al., 2010).

Experimental studies suggest that the main source region for the generation of Archean TTG is strongly controlled by Sr, Y and REE contents, once these elements are very pressure sensitive, therefore their concentrations in the melt depend on the depth and temperature conditions of partial melting (Moyen and Stevens, 2011; Moyen and Martin, 2012). On Sr/Y vs. Y (ppm), $(Yb)_N$ vs. $(La/Yb)_N$, and binary plots the Riacho das Lajes Suite samples represent TTG magmas derived from basaltic oceanic crust that likely experienced high pressure conditions (eclogitic source; Figs. 15a and 15b). Moreover, the $(Gd/Er)_N$ vs. MgO binary plot also suggests a garnet-rich mafic source (Fig. 15c).

Halla et al. (2009) divided the TTG series in two main groups: 1) high-HREE TTGs (low Al), which are related to a garnet-free source, and 2) low-HREE TTGs (high Al), which are related to a garnet-bearing source. According to these authors, such contrasting sources can be attributed to two distinct pressure conditions (1.0 GPa for the first group and > 2.0 GPa for the second one). They also conclude that the involved physical conditions require that the precursor mafic source must be somehow introduced deep into the mantle. Most of the studied samples of Riacho das Lajes Suite are characterized by high $SiO_2$ (> 70 wt.%), $Al_2O_3$ (> 14 wt.%) and Sr (> 350 ppm) contents, in addition to low MgO (< 1 wt.%) and HREE contents, which fits the High-Al low-HREE TTG group (Fig. 15d). These features can be associated to high-pressure and temperature conditions of partial melting of a garnet-rich basaltic (eclogitic) source as predicted by Moyen and Martin (2012) and Martin et al. (2014). Additionally, slightly negative and positive εNd(t) values suggest that these magmas experienced little contribution from the continental crust during their ascent.

Generation of TTG is generally related to the melting of oceanic crust or plateaus in subduction zones (Drummond and Defant 1990; Martin et al., 2005, 2014), melting of an oceanic plateau above a mantle plume (Zegers and van Keken, 2001; Willbold et al., 2009), and interactions between subduction zones and upwelling mantle plumes (Johnson et al., 2013). Thus, we suggest that deep, intraoceanic, hot subduction took place in the Neoarchean (ca. 2.6 Ga), probably underneath an oceanic plateau or protocrust as suggested by results from experimental studies (Halla et al., 2009; Moyen, 2011; Laurent et al., 2014). Partial melting of the slab resulted in a garnet-rich residuum and produced low-HREE TTG melts that generated the granitoid rocks of the Riacho das Lajes Suite (Fig. 17a).

[Fig. 15 near here]

*5.1.2. Floresta Suite*

Metagranitoids and orthogneisses of the ca. 2.1 Ga Floresta Suite display a wide spectrum of $SiO_2$ and CaO values that correspond to the calcic to calc-alkalic series. In addition, they represent highly magnesian magmas with metaluminous to slightly peraluminous character. Samples are characterized by LILE enrichment and HFSE depletions, especially in Nb, P and Ti. This pattern is generally related to the accumulation of Ti-rich phases (e.g., rutile, titanomagnetite and sphene). Furthermore, they exhibit moderate to high REE fractionation, which can be explained by the retention of HREE by garnet in the source region, similar to that in the Riacho das Lajes Suite. Positive Eu peak is observed in most of the samples and is interpreted as resulting from the high concentration of this element in plagioclase during magma crystallization. Eu negative peaks are also present and reflect retention of this element by the same mineral during magma differentiation.

This geochemical signature is typical of magmas generated in subduction-related tectonic settings (Pearce and Peate, 1995; Tatsumi, 2005, Foley et al., 2000; Klemme et al., 2006). Magma generation can be explained by successive episodes of mantle wedge partial melting, which is metasomatized by fluids released from the subducted oceanic plate (Tatsumi, 1989; Scmhidt et al., 2004; Li et al., 2009). Such arc-related magmas rise rapidly to the crust where they undergo fractional crystallization (Sisson and Grove, 1993; Grove et al., 2003). The tectonic discriminant diagram of Pearce (1984, Fig. 16a) also confirms the proposed tectonic setting, whereas the major and trace element signature points out to an igneous high-K mafic source, with small contributions from metasedimentary sources (Fig. 16b).

Some samples are characterized by high concentrations of Ni (>15 ppm), Cr (>20 ppm) and V (> 100 ppm), as well as Ba (> 1000 ppm) and Sr (> 500 ppm). This enrichment of crustal- and mantle-related elements suggests that part of the rock samples from the Floresta Suite is chemically similar to the high-Mg dioritic magmas or sanukitoids (Shirey and Hanson 1984; Stern et al., 1989; Martin et al., 2005, 2010). Experimental studies indicate that such anomalous concentration of these elements rely on the interaction between mantle peridotite and melts enriched in incompatible elements (Halla et al., 2009; Heilimo et al., 2010; Oliveira et al., 2011; Laurent et al., 2014 Semprich et al., 2015). Hence, it seems that the source region for rocks of the Floresta Suite is strongly heterogeneous and the nature of each individual melting origin is still difficult to explain at this time.

The mixing of sources is also reflected by high variability of εNd(t) values calculated for the 2.09 Ga crystallization age. They range from positive to strongly negative, and thus reflect strong input of juvenile material as well as an important crustal component. Negative εNd(t) values also suggest an enriched source (Menzies et al., 1987), which can also be an explanation for the enrichment of transition elements in subduction-related magmas (Halla et al., 2009; Laurent et al., 2014).

Any tectonic scenario for the generation of the Floresta Suite must account for input from crust and metasomatized mantle. The most common tectonic setting for such rocks involves crustal thickening by terrane accretion, which is generally coeval with slab breakoff events, where the retreat of the slab and lithospheric delamination provide an important heat source (Halla et al., 2009; Laurent et al., 2014). Based on the obtained geochemical and isotopic data, we suggest that subduction took place at 2.1-2.0 Ga Ga and resulted in the emplacement of the Floresta Suite (Fig. 17b). This hypothesis is consistent with the description of several accretion events in the region during the Rhyacian period (2.15 to 2.0 Ga, Santos et al., 2013; Santos et al., 2015a; Neves et al., 2015).

[Fig. 16 near here]

[Fig. 17 near here]

### *5.2. Neoarchean crustal growth, Paleoproterozoic reworking and regional correlations*

U-Pb and Sm-Nd data of the TTG rocks of the Riacho das Lajes Suite indicate juvenile magmatism with little crustal contamination at 2.6 Ga in the Borborema Province. This is the first evidence of Archean crust in the Central Subprovince. These rocks present $T_{DM}$ model ages that are very close to the crystallization age and slightly negative to positive εNd(t) values. Therefore, they represent an important continental crustal growth event in the region, although evidence for some crustal contaminantion is also recorded. Dated samples from the Floresta Suite present Rhyacian crystallization ages (~2.1 Ga), and Nd $T_{DM}$ model ages range from Archean to Paleoproterozoic, which suggests mixing of older and younger contributions in the source. These data indicate that crustal growth in the Rhyacian was coeval with reworking of the older Neoarchean crust, in addition to inferred mantle metasomatism. An important parameter related to the emplacement of rocks of the Floresta Suite is that negative εNd (t) values are concentrated in the rims of the intrusion, whereas positive values are present in its core. This strongly suggests that crustal contamination took place mostly in the peripheral region of the intrusion, triggered by country rocks.

It has been suggested that continental growth has been episodic throughout Earth´s history, with main events marked by peaks at 3.3, 2.7, 1.9 and 1.2 Ga (Condie and Kröner, 2013; Brown, 2009; Hawkesworth et al., 2010; Cawood et al., 2013). Moreover, in several cratonic blocks worldwide, the main growth episodes in the Archean took place at approximately 2.7 Ga (Bleeker, 2003). However, although less frequently, juvenile TTGs dated at 2.6 Ga, such as for the Riacho das Lajes, have been documented in the Yilgarn Craton in West Australia (Griffin et al., 2004) and in the North China Craton in China (Wang and Liu, 2012), which suggests that subduction-related events and crustal accretion continued until the Neoarchean-Paleoproterozoic transition, at least in some continental margins (Condie, 2000; Laurent et al., 2014).

Nevertheless, the recognition of such Archean and Paleoproterozoic crustal fragments within younger provinces, such as the Borborema Province, remains a difficult challenge, primarily because of the intense crustal reworking by younger tectonic events. Most of the Archean domains concentrated in the northern portion of the province are interpreted as part of ancient far-travelled terranes or basement inliers, such as the São José do Campestre Massif (Dantas et al., 2013; Souza et al., 2016), Tróia Massif (Costa et al., 2015; Ganade de Araujo et al., 2017) and Granjeiro Terrane (Delgado et al., 2003; Silva et al., 2014). Late Archean associations in these domains have ages in the 2.8-2.7 Ga interval and are a record of juvenile and reworked crust, such as the quartz-dioritic to syenogranitic rocks of the São José do Campestre Terrane and the orthogneisses and granitoids of the Cruzeta Complex of the Tróia Massif (Fetter et al., 2000). Similarity of ages and sources for these Archean successions suggest they may have been linked by the Late Archean.

Possible correlatives of the Riacho das Lajes Suite occur in neighboring cratons. For instance, Neoarchean crustal growth followed by Paleoproterozoic reworking has been documented in the juvenile and reworked mafic-ultramafic sequences, grey gneisses, migmatites and granitic rocks of the Serrinha and Jequié Blocks and Contendas Mirante Belt in the São Francisco Craton (Teixeira et al., 2000; Barbosa and Sabaté, 2005; Oliveira et al., 2011; Romano et al., 2013; Farina et al., 2015). Lastly, Rhyacian orthogneisses are widespread in the inner domains of the Borborema Province as basement rocks. For instance, recent geochronological and geochemical investigation conducted by Neves et al., (2015), has demonstrated that calc-alkaline rocks aged at 2.1 Ga occur through the Central Domain of the Borborema Province, including the Rio Capibaribe Terrane, such as the Vertentes Complex, indicating that these domains may have been connected during that time. Such domains also finds continuity in the African continent, being resulted of the Paleoproterozoic the long-lived Eburnean orogeny (Hein, 2010; Baratoux et al., 2011; Blocks et al., 2014).

### *5.3. Tectonic evolution of the Alto Moxotó Terrane and implications for supercontinent reconstructions*

Previous geodynamic hypotheses on the evolution of the Alto Moxotó Terrane did not consider tectonic events older than the Siderian (2.5-2.3 Ga, Santos et al., 2004; Santos et al., 2015a). However, several inherited zircon grains with ages around 2.7 to

2.6 Ga and associated Archean Nd $T_{DM}$ model ages of the Siderian and Rhyacian units strongly indicate the formation of older crust (Santos et al., 2015a). Nevertheless, available isotopic data concerning crustal events between 2.4 and 2.2 Ga in the Alto Moxotó Terrane are rather scarce. The absence of data over this large time span hampers formulation of major geodynamic models or establishing accurate correlations. A synthesis of available isotopic data plus the results of this study is presented in Fig. 18.

In the present study, we suggest that the evolution of the Alto Moxotó Terrane began with a subduction-related event in the Neoarchean (ca. 2.6 Ga), which involved the melting of oceanic basaltic crust in an intra-oceanic setting that produced the TTG magmas of the Riacho das Lajes Suite. Subsequently, this geodynamic scenario may have evolved to cratonized crust or microcontinent in the early Paleoproterozoic that may have been the source of several inherited Archean zircon grains found in other Paleoproterozoic units (Santos et al., 2015a). Between 2.2 and 2.0 Ga, arc accretion took place within a continental magmatic arc context and produced mafic-ultramafic tholeiitic magmas that evolved to calc-alkaline magmas (Santos et al., 2015b; Neves et al., 2015). Peraluminous gneisses formed at approximately 2.0 Ga indicate a final continental collision marking the end of this convergent cycle, and resulted in high-grade metamorphism (see Santos et al., 2015a and Neves et al., 2015 for details).

Several authors stated that most of cratonic fragments or microcontinents are missing in Paleoproterozoic supercontinent reconstructions, which may be represented by basement inliers or exotic terranes that occur within younger orogenic belts (e.g. Reddy and Evans, 2009; Bradley, 2011). In this sense, the recognition of old crustal segments, such as the Alto Moxotó Terrane within the Neoproterozoic Borborema Province, may provide useful information to understanding the evolution of Paleoproterozoic supercontinents such as Nuna and Atlantica (Rogers and Santosh 2004; Zhao et al., 2002, 2004).

[Fig. 18 near here]

## 6. Conclusions

The main obtained results of this paper can be summarized as:

(1) In the westernmost Alto Moxotó Terrane, Borborema Province, NE Brazil, we identified two distinct metaplutonic suites that represent important Neoarchean (ca. 2.6 Ga) and Rhyacian (ca. 2.1 Ga) tectono-magmatic events;

(2) Emplacement of the high-Al low-REE TTG Riacho das Lajes Suite is the first record of Neoarchean rocks within the Central Subprovince of the Borborema Province. Its rock association was generated in a garnet-rich and fluid-absent source, which points to slab melting of oceanic crust metamorphosed under eclogite facies conditions. Nd isotopes clearly indicate a juvenile source with only minor crustal contamination. We interpret this event as the result of subduction beneath a thick oceanic plateau/protocrust;

(3) Emplacement of the Floresta Suite tonalites, granodiorites and granites represents the Paleoproterozoic event (ca. 2.1 Ga). Geochemical parameters are compatible with subduction-related magmas. Combined trace-element geochemistry and isotopic data indicate a heterogeneous source, involving K-rich mafic rocks and minor contributions of metasedimentary deposits. Mantle metasomatism likely also took place. Heterogeneity is also reflected in the distribution of $\varepsilon Nd(t)$ values, suggesting major involvement of country rocks, particularly in the marginal zones of the intrusions. The Floresta Suite records both juvenile magmatism and intense crustal reworking of Archean to Paleoproterozoic crust. We suggest that the Rhyacian (ca. 2.1 Ga) accretion of terranes resulted in the emplacement of the Floresta magmas, coeval with slab breakoff. Slab retreat and lithospheric delamination provided the heat source. This interpretation is consistent with several subduction-related events suggested for this period in the Borborema Province.

(4) Although the major Neoarchean crustal growth events have been dated at 2.7 Ga in several provinces worldwide, magmatism extended until 2.6 and 2.5 Ga, as recorded in the Riacho das Lajes Suite of the Alto Moxotó Terrane. Accretion of Rhyacian (ca. 2.1 Ga) magmatic arc was widespread in most Paleoproterozoic cratonic blocks, including the São Francisco-Congo Craton, where they are interpreted as being related to the Transamazonian-Eburnean orogeny.

## 7. Acknowledgements

This paper is the outcome of the first author PhD thesis at Universidade de Brasília, Brazil. Authors are thankful to Universidade de Brasília geochronology lab staff. Esa Heilimo (Geological Survey of Finland) revised a previous manuscript version. ELD and RAF acknowledge CNPq financial support through INCT Estudos Tectônicos and research fellowships. PAC was supported by Australian Research Council grant FL160100168. We are also grateful to W.R. Van Schmus and S.P. Neves for helpful comments and suggestions that considerably improved the original MS, as well as the efforts of James Kellog and Kerry McCarnet-Castle.

## 8. References

Almeida, F.F.M., Hasui, Y., Brito Neves, B.B., Fuck, R.A., 1981. Brazilian structural provinces: an introduction. Earth Science Reviews 18, 1-29.

Archanjo, C.J., Hollanda, M.H.B.M., Rodrigues, S.W., Brito Neves, B.B., 2008. Fabrics of pre- and syntectonic granite plutons and chronology of shear zones in the Eastern Borborema Province, NE Brazil. Journal of Structural Geology 30, 310-336.

Archanjo, C.J., Viegas, L.G., Freimann, Hollanda, M.H.B.M. 2013. O Lineamento Patos: Estrutura e evolução. In: 25º Simpósio de Geologia do Nordeste, Proceedings, pp. 481 482.

Arndt, N.T., 2013. Formation and evolution of the Continental Crust. Geochemical Perspectives (European Association of Geochemistry) 2, 405-533.

Ávila, C.A., Teixeira, W., Cordani, U.G., Moura, C.A.V., Pereira, R.M., 2010. Rhyacian (2.23–2.20 Ga) juvenile accretion in the southern São Francisco craton, Brazil: geochemical and isotopic evidence from the Serrinha magmatic suite, Mineiro Belt. Journal of South American Earth Sciences 29, 464–482.

Baratoux, L., Metelka, V., Naca, S., Jessel, M.W., Gregoire, M., Ganne, J., 2011. Juvenile Paleoproterozoic crust evolution during the Eburnean orogeny (2.20 - 2.0 Ga), western Burkina Faso. Precambrian Research 191-18-45.

Barbosa, J.S.F., Sabaté, P. 2004. Archaean and Paleoproterozoic crust of the São Francisco Craton, Bahia, Brazil: Geodynamic features. Precambrian Research 133, 1–27.

Barker, F., Arth, J.G., 1976. Generation of trondhjemite-tonalite liquids and Archean bimodal trondhjemite-basalt suites. Geology 4, 596–600.

Bleeker, W., 2003. The late Archean record: a puzzle in ca. 35 pieces. Lithos, 71, 99-134.

Blocks, S., Ganne, J., Baratoux, L., Zeh, A., Parra-Avila, L.A., Jessel, M., Ailleres, L., Siebenaller, L., 2015. Petrological and geochronological constraints on lower crust exhumation during Paleoproterozoic (Eburnean) orogeny, NW Ghana, West African Craton. Journal of Metamorphic Petrology 33, 436-494.

Bradley, D.C., 2011. Secular trends in the geologic record and the supercontinent cycle: Earth and Planetary Science Letters 108, 16–33.

Brito Neves, B.B., 1975. Regionalização Geotectônica Do Précambriano Nordestino (Phd thesis). Universidade de São Paulo, São Paulo, p. 198.

Brito Neves, B.B., 2011. The Paleoproterozoic in the South American continent: diversity in the geologic time. Journal of South American Earth Sciences 32, 270-286.

Brito Neves, B.B., Santos, E.J., Schmus, W.R.Q., 2000. Tectonic history of the Borborema Province. In: Umberto Cordani; Edson José Milani; Antonio Thomaz Filho; Diogenes de Almeida Campos (Org.). Tectonic Evolution of South America. Rio de Janeiro: 31st International Geological Congress, pp. 151-182. Special Publication.

Brito Neves, B.B., Van Schmus, W.R., Santos, E.J., Campos Neto, M.C., Kozuch, M., 2005. O Evento Cariris Velhos na Província Borborema: integração de dados, implicações e perspectivas. Revista Brasileira de Geociências 25, 279-296.

Brito Neves, B.B., Sproesser, W.M., Petronilho, L.A., Souza, S.L., 2013. Contribuição a geologia e geocronologia do Terreno Rio Capibaribe (TRC, Província Borborema). Geologia USP - Série Científica 13, 97-122.

Brito Neves, B.B., Fuck, R.A., Pimentel, M.M.  2014. The Brasiliano collage in South America: a review. Brazilian Journal of Geology 44, 493-518.

Brown, M., 2009. Metamorphic patterns in orogenic systens and the geological record. in: P.A. Cawood, A. Cawood, A. Kröner (Eds.), Accretionary Orogens in Space and Time, Geological Society, London, Special Publications, vol. 318 (2009), pp. 37–74.

Bühn, B.M., Pimentel, M.M., Matteini, M., Dantas, E.L., 2009. High spatial resolution analysis of Pb and U isotopes for geochronology by laser ablation multicollector inductively coupled plasma mass spectrometry (LA-MC-ICP-MS). Anais da Academia Brasileira de Ciências 81, 1-16.

Castillo, P.R., 2006. An overview of adakite petrogenesis. Chinese Science Bulletin 51, 257-268.

Caxito, F.A., Uhlein, A., Dantas, E.L. 2014a. The Afeição augen-gneiss suíte and the recorf of the Cariris Velhos Orogeny (1000-960 Ma) within the Riacho do Pontal fold belt, NE Brazil. Journal of South American Earth Sciences 51, 12-27.

Caxito, F.A., Uhlein, A. Ross, S., Uhlein, G.J. 2014b. Neoproterozoic oceanic crust remmants in northeast Brazil. Geology 42, 387-390.

Cavoise, A.J., Valley, J.W., Wilde, S.A., 2006. Correlated micro-analysis of zircon: trace element, d18O and U-Th-Pb isotopic constraints on the igneous origin of complex > 3900 Ma detrital grains. Geochemica et Cosmochimica Acta 70, 5601-5616.

Cawood, P.A., Hawkesworth, C.J., Dhuime, B., 2013. The continental record and the generation of continental crust. Geological Society of America Bulletin 125, 14-32.

Condie, K.C., 1998. Episodic continental growth and supercontinents: a mantle avalanche connection? Earth and Planetary Science Letters 163, 97-108.

Condie, K.C., 2000. Episodic continental growth models: afterthoughts and extensions. Tectonophysics 322, 153–162.

Condie, K.C., 2005. TTGs and adakites: are they both slab melts? Lithos 80, 33–44.

Condie, K.C., Kröner., 2013. The building blocks of continental crust: Evidence for a major change in tectonic setting of continental growth at the end of the Archean. Gondwana Research 23, 394-412.

Coney, P.J., Jones, D.L., Monger J.W.H., 1980. Cordilleran suspect terranes. Nature 288, 329-333.

Costa, F.G., Palheta, E.S.M., Rodrigues, J.B., Gomes, I.P.G., Vasconcelos, A.M. 2015. Geochemistry and U-Pb zircon ages of plutonic rocks from the Algodões granite-greenstone terrane, Troia Massif, northern Borborema Province, Brazil: Implications for Paleoproterozoic subdiction-accretion processes. Journal of South American Earth Sciences 59, 45-68.

Dantas, E.L., Souza, Z.S., Wernick, E., Hackspacher, P.C., Martin, H., Xiadong, D., Li, J.W., 2013. Crustal growth in the 3.4-2.7 Ga São José do Campestre Massif, Borborema Province, NE Brazil. Precambrian Research 227, 12-156.

Davies, J.H., von Blanckerburg, F., 1995. Slab breakoff: a model of lithospheric detatchment and its test in the magmatism and deformation of collisional orogens. Earth and Planetary Science Letters 129, 85-102.

De Wit, M.J., Stankiewicz, J., Reeves, C., 2008. Restoring Pan-African-Brasiliano connections: more Gondwana control, less Trans-Atlantic corruption. In: Pankhurst, R.K., Trouw, R.A.J., Brito Neves, B.B., De Wit, M.J. (Eds.), West Gondwana: Pre-Cenozoic Correlations Across the South Atlantic Region. Geological Society Special Publication 294, London, pp. 399-412.

Delgado, I.M., Souza, J.D., Silva, L.C., Silveira Filho, N.C., Santos, R.A., Pedreira, A.J., Guimarães, J.T., Angelin, L.A.A., Vasconcelos, A.M., Gomes, I.P., Lacerda Filho, J.V., Valente, C.R., Perrota, M.M., Heineck, C.A. 2003. Geotectônica do Escudo Atlântico: In: Bizzi, L.A., Schobbenhaus, C., Vidotti, R.M., Gonçalves, J.H. (eds). Geologia, Tectônica e Recursos Minerais do Brasil. CPRM, 227-234.

DePaolo, D.J., 1981. A neodymium and strontium isotopic study of the Mesozoic calc-alkaline granitic batholiths of the Sierra Nevada and Peninsular Ranges, California. Journal of Geophysical Researcg. 86, 10470-10488.

Defant, M.J., Drummond, M.S. 1990. Derivation of some modern arc magmas by melting of young subducted lithosphere. Nature 347, 662– 665.

Drummond, M.S., Defant, M.J., 1990. A model for trondhjemite-tonalite-dacite genesis and crustal growth via slab melting: Archean to modern comparisons. Journal of Geophysical Research 95, 21503-21521.

Evans, D.A.D., Mitchell, R.N., 2011. Assembly and breakup of the core of Paleoproterozoic–Mesoproterozoic supercontinent Nuna. Geology 39, 443–446.

Farina, F., Albert, C., Lana, C., 2015. The Neoarchean transition between medium- and high-K granitoids: Clues from the Southern São Francisco Craton (Brazil). Precambrian Research 266, 375-394.

Fetter, A.H., Van Schmus, W.R., dos Santos, T.J.S., Nogueira Neto, J.A., Arthaud, M.H., 2000. U-Pb and Sm-Nd geochronological constraints on the crustal evolution and basement architeture of Ceará State, NW Borborema Province, NE Brazil: implications for the existence of the Paleoproterozoic supercontinent Atlantica. Revista Brasileira de Geociências 30, 102-106.

Fetter, A.H., Santos, T.J.S., Van Schmus, W.R., Hackhpacher, P.C., Brito Neves, B.B., Arthaud, M.H., Nogueira Neto, J.A., Wernick, E. 2003. Evidence for Neoproterozoic continental arc magmatism in the Santa Quiteria Batholith of Ceará State, NW Borborema Province, NE Brazil: implications for the assembly ofWestern Gondwana. Gondwana Research 6, 265-273.

Foley, S.F., Barth, M.G., Jenner, G.A., 2000. Rutile/melt partition coefficient for trace elements and an assesment of the influence of rutile on the trace element characteristics of subduction zone magmas. Geochemistry at Cosmochimica Acta 64, 933-938.

Frost, B.R., Barnes, C.G., Collins, W.J., Arculus, R.J., Ellis, D.J., Frost, C.D., 2001. A geochemical classification of granitic rocks. Journal of Petrology 42, 2033–2048.

Ganade de Araújo, C.E., Weinberg, R.F., Cordani, U.G., 2014a. Extruding the Borborema Province (NE-Brazil): a two-stage Neoproterozoic collision process. Terra Nova 26, 157-168.

Ganade de Araujo, C.E., Cordani, G.U., Weinberg, R., Basei, M.A.S., Armostrong, R., Sato, K. 2014b. Tracing Neoproterozoic subduction in the Borborema Province (NE-Brazil): clues from U-Pb geochronology and Sr-Nd-Hf-O isotopes on granitoids and migmatites. Lithos 202-203, 167-189.

Ganade de Araujo, C.E, Rubatto, D., Hermann, J., Cordani, G.U., Caby, R., Basei, M.A.S. 2014c. Ediacaran 2,500 km-long synchronous deep continental subduction in the Western Gondwana Orogen. Nature Communications 1, 1-8.

Ganade de Araujo, C.E., Basei, M.A.S., Grandjean, F.C., Armstrong, R., Brito, R.S.C., 2017. Contrasting Archean (2.85-2.68 Ga) TTGs from the Tróia Massif (NE-Brazil) and their geodynamic implications for flat to steep subduction transition. Precambrian Research 297, 1-18.

Gióia, S.M.C.L., Pimentel, M.M., 2000. The Sm-Nd isotopic method in the geocrhronology laboratory of the University of Brasilia. Anais da academia brasileira de ciências 72, 219-245.

Griffin W.L., Belousova, E.A., Shee, S.R., Pearson, N.J., O´Reilly, S.Y., 2004. Archean crustal evolution in the northern Yilgran Craton: U-Pb and Hf-isotope evidence from detrital zircons. Precambrian Research 2004, 231-282.

Halla, J., can Hunen, J.,, Heilmo E., Hottla, P., 2009. Geochemical and numerical constraints on Neoarchean plate tectonics. Precambrian Research 175, 155-162.

Hawckesworth, C.J., Dhuime, B., Pietranik, A.B., Cawood, P.A., Kemp., A.I.S., Storey, C.D., 2010. The generation and evolution of the continental crust. Journal of the Geological Society 167, 229-248.

Hein, K.A.A., 2010. Succession of structural events in the Goren greenstone belt (Burkina Faso): Implications for West African tectonics. Journal of African Earth Sciences 58, 83-94.

Heilimo, E., Halla, J., Hölttä, P., 2010. Discrimination and origin of the sanukitoid series: geochemical constraints from the Neoarchean western Karelian Province (Finland). Lithos 115, 27–39.

Hollister, L.S., Andronicos, C.L., 2006. Formation of new continental crust in Western British Columbia during transpression and transtension. Earth and Planetary Science Letters 249, 29-38.

Jackson, S.E., Pearson, N.J., Griffin, W.L., Belousova, E.A., 2004. The application of laser ablation-inductively coupled plasma-mass spectrometry to in situ U–Pb zircon geochronology. Chemical Geology 211, 47–69.

Johnson, T., Brown, M., Kaus, B.J.P., van Tongeren, J.A., 2013. Delamination and recycling of Archaean crust caused by gravitational instabilities. Nature Geoscience 7, 47–52.

Kelley, A.K., Plank, T., Newman, S., Stolper, E.M., Grove, T.L., Parman, S., Hairu, E.H., 2010. Mantle melting as a function of water content beneath the Mariana Arc. Journal of Petrology 51, 1711-1738.

Klemme, S., Gunther, D., Hametner, K., Prowatke, S., Zack, T., 2006. The partitioning of trace elements between ilmenite, ulvospinel, armalcolite and silicate melts with implications for the early differentiation of the moon. Chemical Geology 234, 251–263.

Kozuch, M., 2003. Isotopic and trace element geochemistry of Early Neoproterozoic gneissic and metavolcanic rocks in the Cariris Velhos Orogen of the Borborema Province, Brazil, and their bearing tectonic setting (PhD thesis). Kansas University, Lawrence, p. 199.

Laurent, O., Martin, F., Moyen, J.F., Doucelance, R., 2014. The diversity and evolution of late-Archean granitoids: Evidence for the onset of "modern-style" plate tectonics between 2.0 and 2.5 Ga. Lithos 205, 208-235.

Lima, M.I.C., Gava, A., Fernandes, P.E.C.A., Pires, J.L., Siga Jr, O., 1985. Projeto titanado de Floresta. Minérios de Pernambuco/Radam Brasil, 314 pp.

Maniar, P.D., Piccoli, P.M., 1989. Tectonic discrimination of granitoids. The Geological Society of America Bulletim 101, 635–643.

Martin, H., 1986. Effect of steeper Archean geothermal gradient on geochemistry of subduction-zone magmas. Geology 14, 753-756.

Martin, H., Smithies, R.H., Rapp, R., Moyen, J.F., Champion, D. 2005. An overview of adakite, TTG and sanukitoid: relationships and some implications for crustal evolution. Lithos 79, 1-24.

Martin, H., Moyen, J.F., Rapp, R., 2010. Sanukitoids and the Archaean-Proterozoicboundary. Transactions of the Royal Society of Edinburgh-Earth Sciences 100, 15–33.

Martins, G., Oliveira, E.P., Lafon, J., 2009. The Algodões amphibolite tonalite gneisse sequence, Borborema Province, NE Brazil: Geochemical and geochronological evidenc for Paleoproterozoic accretion of oceanic plateau/back-arc basalts and adakitic plutons. Gondwana Research 15, 71-85.

Matteinni, M., Junges, S.L., Dantas, E.L., Pimentel, M.M., Buhn, B.M., 2009. In situ zircon U-Pb and Lu-Hf isotope systematic on magmatic rocks: insights on the crustal evolution of the Neoproterozoic Goiás Magmatic Arc, Brasília belt, Central Brazil. Gondwana Reearch. 16, 200-212.

McDonough, W.F., Sun, S.S., 1995. The composition of the Earth. Chemical Geology 120, 223-253.

Menzies, M.A., Rogers, Tindle, A., Hawkesworth, C., 1987. Metasomatic and enrichment processes in lithospheric peridotites, an effect of asthenosphere-litosphere interaction. In: Menzies, M.A., Hawkesworth, C.J. (Eds.), Mantle Metasomatism. Academic press, London, pp. 313-361.

Moyen, J.F., Martin, H., Jayananda, M., Auvray, B., 2003. Late Archaean granites: a typology based on the Dharwar Craton (India). Precambrian Research 127 (1–3), 103–123.

Moyen, J.F., Stevens, G., 2006. Experimental constraints on TTG petrogenesis: implications for Archean geodybamics. In Benn, K., Mareschal, J-c., Condie, K.C. (Eds.) Archean Geodunamics and Environments, AGU, pp. 149-178.

Neves, S.P., 2011. Atlantica revisited: new data and thoughts on the formation and evolution of a long-lived continent. International Geology Review 41, 1377-1391.

Neves, S.P., 2015. Constraints from zircon geochronology on the tectonic evolution of the Borborema Province (NE Brazil): Widespread intracontinental Neoproterozoic reworking of a Paleoproterozoic accretionary orogen. Journal of South American Earth Sciences 58, 150-164.

Neves, S.P., Lages, G.A., Brasilino, R.G., Miranda, A.W.A., 2015. Paleoproterozoic accretionary and collisional processes and the build-up of the Borborema Province (NE Brazil): Geochronological and geochemical evidence from the Central Domain. Journal of South American Earth Sciences 58, 165-187.

Nielsen, R., 2007. Geochemical Earth Reference Model (GERM) partition coefficient (Kd) data base. Avaliable on the website: http://www.geo.oregonstate.edu/people/faculty/nielsenr.htm.

Niu, Y., O´Hara, M.J., 2009. MORB mantle hosts the missing Eu (Sr, Nb, Ta and Ti( in the continental crust: New perspectives on crustal growth, crust mantle differentiation and chemical structure of oceanic upper mantle. Lithos 112, 1-17.

O´Connor, T.J., 1965. A classification for quartz-rich igneous rocks based on feldspar ratios. US Geological Survey Professional Paper 52B, 79-84.

Oliveira, E.P., Souza, Z.S., McNaughton, N., Lafon, J.M., Costa, F.G., Figueiredo, A.M., 2011. The Rio Capin volcanic-plutonic-sedimentary belt, São Francisco Craton, Brazi: geological, geochronological and isotopic evidence for oceanic arc accretion during Paleoproterozoic continental collision. Gondwana Research 19, 735-750.

Pearce, J.A., 1982. Trace elements characteristics of lavas from destructive plate boundaries. In: Thorpe, R.S. (Ed.), Andesites. John Wiley and Sons, London, pp. 525-548.

Pearce, J.A., Harris, N.B.W., Tindle, A.G., 1984. Trace element discrimination diagrams for the tectonic interpretation of granitic rocks. Journal of Petrology 25, 956-983.

Rapp, R.P., Watson, E.B., 1995. Dehydration melting of metabasalt at 8–32 kbar: implications for continental growth and crust– mantle recycling. Journal of Petrology 36, 891–931.

Rapp, R.P., Shimizu, N., Norman, M.D. 2003. Growth of early continental crust by partial melting of eclogite. Nature 425, 605-609.

Reddy, S.M., Evans, D.A.D., 2009, Palaeoproterozoic supercontinents and global evolution: Correlations from core to atmosphere, in Reddy, S.M., et al., eds., Palaeoproterozoic supercontinents and global evolution: Geological Society of London Special Publication 323, p. 1–26.

Rodrigues, S.W.O., Brito Neves, B.B., 2008. Padrões isotópicos Sm-Nd no limite entre os Terrenos Alto Pajeú e Alto Moxotó (PB). Revista Brasileira de Geociências 38, 211-227.

Rogers, J.J.W., Santosh, M., 2002. Configuration of Columbia, a Mesoproterozoic supercontinent. Gondwana Research 5, 5-22.

Rogers, J.J.W. Santosh, M., 2009. Tectonics and surface effects of the supercontinent Columbia. Gondwana Research 15, 373-380.

Romano, R., Lana, C., Alkmin, F.F., Stevens, G.S., Armstrong, R., 2013. Stabilization of the southern portion of the São Francisco Craton, SE Brazil, trough a long lived period of potassic magmatism. Precambrian Research 224, 143-159.

Rudnick, R.L., 1995. Making continental crust. Nature 378, 571-578.

Santos, E.J., 1995. O complexo granítico Lagoa das Pedras: acresção e colisão na região de Floresta (Pernambuco), Província Borborema (PhD thesis). Instituto de Geociências da Universidade de São Paulo, São Paulo, p. 228.

Santos, E.J., 1996. Ensaio preliminar sobre terrenos e tectônica acrecion_aria na Província Borborema. In: SBG, Congresso Brasileiro de Geologia, 39o, Salvador, Proceedings, pp. 47-50.

Santos, E.J., Medeiros, V.C., 1999. Constraints from granitic plutonism on proterozoic crustal growth of the Transverse Zone, Borborema Province, NE-Brazil. Revista Brasileira de Geociências 29, 73-84.

Santos, E.J., Nutman, A.P., Brito Neves, B.B., 2004. Idades SHRIMP U-Pb do Complexo Sertânia: implicações sobre a evolução tectônica da Zona Transversal, Província Borborema. Geol. USP - Série Científica 4, 1-12.

Santos, E.J., Van Schmus,W.R., Kozuch, M., Brito Neves, B.B., 2010. The Cariris Velhos tectonic event in northeast Brazil. J. South Am. Earth Sci. 29, 61-76.

Santos, E.J., Souza Neto, J.A., Carmona, L.C.M., Armostrong, R., Santos, L.C.M.L., Mendes, L.U.S., 2013. The metacarbonate rocks of Itatuba (Paraíba): a record of sedimentary recycling in a Paleoproterozoic collision zone of the Borborema Province, NE Brazil. Precambrian Research 224, 454-471.

Santos, L.C.M.L., Santos, E.J., Dantas, E.L., Lima, H.M., 2012. Análise estrutural e metamórfica da região de Sucuru (Paraíba): Implicações sobre a evolução do Terreno Alto Moxotó, Província Borborema. Geologia USP - Série Científica 12, 5-20.

Santos, L.C.M.L., Dantas, E.L., Santos, E.J., Santos, R.V., Lima, H.M., 2015a. Early to late Paleoproterozoic magmatism in NE Brazil: the Alto Moxoto Terrane and its tectonic implications for the pre-Western Gondwana assembly. Journal of South American Earth Sciences.58, 188-209.

Santos, L.C.M.L., Fuck, R.A., Santos, E.J., Dantas, E.L., 2015b. Análise tectônica de terrenos: metodologia, aplicação em cinturões orogênicos e exemplo das províncias Tocantins e Borborema, Brasil. Geonomos 22, 51-63.

Santos, R.V., Santos, E.J., Souza Neto, J.A., Carmona, L.C.M., Sial, A.N., Mancine, L.H., Santos, L.C.M.L., Nascimento, G.H., Mendes, L.U.D.S., Anastacio, E.M.F., 2012b. Isotope geochemistry of Paleoproterozoic metacarbonates from Itatuba, Borborema. Province, Northeastern Brazil: evidence of marble melting within a collisional suture. Gondwana Research 21, 1-13.

Semprich, J., Moreno, J.A., Oliveira, E.P., 2015. Phase equilibria and trace element modeling of Archean sanukitoid melts. Precambrian Research 269, 122-138.

Shaw, D.M., 1970. Trace element fractionation during anatexis. Geochimica and Cosmochimica Acta 34, 237–243.

Shirey, S.B., Hanson, G.N., 1984. Mantle-derived Archaean monzodiorites and trachyandesites. Nature 310, 222-224.

Silva, L.C., Costa, F.G., Armstrong, R., McNaughton, N.J., 2014. U-Pb (SHRIMP) zircon dating and Nd isotopes at basement inliers from Northern Borborema Province, Ceará State, NE Brazil: evidences for the Archean and Paleoproterozoic crustal evolution. In: 9th South American Symposium on Isotope Geology, São Paulo, Brazil, p. 175.

Smithies, R.H., Champion, D.C. 2000. The Archean high-Mg diorite suite: links to Tonalite-Trondhjemite-Granodiorite magmatism and implications for Early Archean crustal growth. Journal of Petrology 41, 1653–1671.

Souza, Z.S., Kalsbeek, F., Deng, X.D., Frei, R., Kokfelt, E.T., Dantas, E.L., Wei, J-W., Pimentel, M.M., Galindo, A.C., 2016. Generation of continental crust in the northern part of the Borborema Province, northeastern Brazil, from Archaean to Neoproterozoic. Journal of South American Earth Sciences 68, 68-96.

Stern, R.A., Hanson, G.N., 1991. Archaean High-Mg granodiorites: a derivative of light rare earth enriched monzodiorites of mantle origin. Journal of Petrology 32, 201–238.

Streckeisen, A.L., 1976. To each plutonic rocks its proper name. Earth Science Reviews 12, 1–33.

Sylvester, P.J., 1994. Archaean granite plutons. In: K.C. Condie (Ed.), Archaean crustal evolution, developments in Precambrian Geology. V. 11, Elsevier, Amsterdam, pp. 261-314.

Tatrumi, Y., Eggins, S. 1995. Subduction Zone Magmatism. Blackwell Science, Oxford, UK.

Teixeira, W., Sabaté, P., Barbosa, J.S.F., Noce, C.M., Carneiro, M.A. 2000. Archean and Paleoproterozoic Tectonic evolution of the São Francisco Craton, Brazil. In: Cordani, U.G., Milani, E.J., Thomas Filho, A., Campos, D.A. (Eds.), Tectonic Evolution of the South America. In: Int. Geol. Congr. 31, Rio de Janeiro, pp. 101–137.

Trompette, R., 1994. Geology of Western Gondwana, Pan African-Brasiliano Aggregation of South America and Africa. A.A. Balkema, Rotterdam, p. 350.

van Keken, P.E., Kiefer, B., Peacock, S.N. 2002. High-resolution models of subduction zones: Implications for mineral dehydratation reactions and the transport of water into the deep mantle. Geochemistry, Geophysics and Geosystems 3, 1-10.

Van Schmus, W.R., Brito Neves, B.B., Hackspacher, P.C., Babinski, M., 1995. U/Pb and Sm/Nd geochronologic studies of the eastern Borborema Province, Northeast Brazil: initial conclusions. Journal of South American Earth Sciences 8, 267-288.

Van Scmmus, W.R., Oliveira, E.P., Silva Filho, A.F., Toteu, F., Penaye, J., Guimarães, I.P., 2008. Proterozoic links between the Borborema Province, NE Brazil, and the Central African Fold Belt. Geological Society of London Special Publication 294, 66-69.

ACCEPTED MANUSCRIPT

Van Schmus, W.R., Kozuch, M., Brito Neves, B.B., 2011. Precambrian history of the Zona Transversal of the Borborema Province. Joutnal of South American Earth Sciences 31, 227-252.

Vauchez, A. Neves, S.P., Caby, R., Corsini, M., Egydio-Silva, M., Arthaud, M., Amaro, V.E., 1995. The Borborema shear zone system, NE Brazil. Journal of South American Earth Sciences 8, 247-266.

Wan, Y.S., Xie, S.W., Yang, C.H., Kröner, A., Ma, M.Z., Dong, C.Y., Di, L.L., Xie, H.Q., Liu, D.Y. 2014. Early Neoarchean (~2.7 Ga) tectono-thermal events in the North China Craton: a synthesis. Precambrian Research, 247, 45-63.

Wang, A., Liu, Y., 2012. Neoarchean (2.5–2.8 Ga) crustal growth of the North China Craton revealed by zircon Hf isotope: A synthesis. Geoscience Frontiers 3, 147-173.

Zegers, E.T., van Keken, P.E., 2001. Middle Archean continent formation by crustal delamination. Geology 29, 1038-1086.

Zhao, G., Cawood, P.A., Wilde, S.A., Sun, M., 2002. Review of global 2.1-1.8 Ga orogens: implications for a pre-Rodínia supercontinent. Earth Science Reviews 59, 125-162.

Zhao, G.C., Suna, M., Simon, A.W., Sanzhong, L., 2004. Paleo-Mesoproterozoic supercontinent: assembly, growth and breakup. Earth Science Reviews 67, 91-123.

**FIG. CAPTIONS**

Fig. 1 - Geodynamic context of the Borborema Province in pre-drift reconstruction for West Africa and northeastern South America, b) tectonic framework of the Borborema Province and c) Simplified geological map of the Central Subprovince and its terranes with the study area highlighted.

Fig. 2 – Geological map of the Airi area with the location of the Riacho das Lajes and Floresta suites. PEL = Pernambuco Lineament, SJN = Serra de Jabitacá Nappe. The red circles of Floresta and Airí represents the main towns of the area.

Fig. 3 – Field aspects of metaplutonic studied rocks. a) Discretely foliated metagranitoid (Riacho das Lajes suite); b) Biotite gneiss with well developed compositional banding (Riacho das Lajes suite); c) Stromatic metatexite with tonalitic protolith (Riacho das Lajes suite); d) Metagranitoid with granodioritic composition (Floresta suite); e) Coarse-grained metatonalite (Floresta Suite); e) Compositional banding of tonalitic to granodioritic orthogneiss (Floresta Suite).

Fig. 4 – Modal composition of studied samples from Riacho das Lajes and Floresta suites reported in the Q-A-P triangular diagram from Streckeisen (1976).

Fig. 5 – Photomicrographs of the studied rocks (a to e = crossed nicols and f = parallel nicols). a) Hypidioblastic granular texture in metatonalite (Riacho das Lajes Suite); b) Granoblastic texture exhibiting deformed qtz grains in metagranodiorite (Riacho das Lajes Suite); c) Elongated biotite within quartz-plagioclase aggregates in metagranodiorite (Riacho das Lajes Suite); d) and e) Graboblastic texture in metatonalite and metadiorite, respectively (Floresta Suite), f) Greenish hornblende aggregates in metagranitic rock (Floresta Suite).

Fig. 6 - Geochemical characteristics of the Riacho das Lajes and Floresta suites. a) Normative An-Ab-Or triangle (O´Connor, 1965); b) $SiO_2$ vs. $Na_2O + K_2O - CaO$ diagram (Frost et al. 2001); c) SiO2 vs. FeOt/(FeOt + MgO) diagram (Frost et al. 2001); d) $Al_2O_3/(Na_2O + K_2O)$ molar vs. $Al_2O_3/CaO + Na_2O + K_2O)$ molar diagram (Maniar and Picolli, 1989); e) Cationic Ca-Na-K diagram showing classical calc-alkaline and trondhjemitic (Barker and Arth, 1976) evolutions.

Fig. 7 - a) Spider diagrams of trace elements abundances; b) REE abundances for rocks of the Riacho das Lajes Suite, 1995; c) Spider diagrams of trace elements abundances and b) REE abundances for rocks of the Floresta Suite. Spiderdiagrams were normalized by primitive mantle from Mcdonough and Sun, 1995 and REE normalized by Chondrite from Nakamura (1974). Black circles = Riacho das Lajes Suite, Red circles = Floresta Suite.

Fig. 8 - Selected cathodoluminescene images of analyzed zircons for U-Pb geochronology.

Fig. 9 – U-Pb zircon age of metatonalite from the Riacho das Lages Suite (Sample FL-56).

Fig. 10 – U-Pb zircon age for a metagranodiorite of the Riacho das Lajes Suite (sample FL-105).

Fig. 11 – U-Pb Concordia diagram for a metadiorite of the Floresta suite (sample FL-65).

Fig. 12 – U-Pb Concordia diagram for a metatonalite of the Floresta suite (sample FL-60).

Fig. 13 - Distribution of obtained Nd data along the Riacho das Lajes and Floresta Suites. The white circles represent the location of selected samples for U-Pb analysis. White circles represent the U-Pb dated samples.

Fig. 14 – Nd evolution diagram for the metaplutonic rocks of a) Riacho das Lajes and b) Floresta Suites.

Fig. - 15 - Plots for the Riacho das Lajes Suite: a) Sr/Y diagram with fields of Archean TTG and adakites and normal calc-alkaline rocks from Drummond and Defant (1990) and b) (La/Yb)n vs. $(Yb)_N$ diagram. Fields of Archean TTG and post-Archean granitoids are from Martin (1986). Partial melting curves of eclogites, garnet amphibolites and amphibolites were calculated using the batch melting equation of Shaw (1970) and the partition coefficients compiled Rollinson (1993) and Nielsen (2007); c) (Gd/Er)n vs. MgO diagram with fields of low- to high HREE TTG and sanukitoids and hypothetic source end-members of garnet-bearing or garnet-free basaltic crust or mantle (high MgO) from Halla et al. (2009); d) $Al_2O_3$ vs. $SiO_2$ diagram separating low- and high HREE groups from Halla et al. (2009).

Fig. 16 - Plots for the Floresta Suite: a) Discriminant tectonic digram after Pearce et al. (1984); b) $Al_2O_3$/(FeOt+MgO) - 3CaO-5($K_2O$/$Na_2O$) plot with fields after Laurent et al. (2014).

Fig. 17 - Sketch tectonic model with suggested scenarios for Riacho das Lajes (a) and Floresta suite (b) magma emplacements.

Fig. 18 - Synthesis of obtained Nd data for rocks of the Alto Moxotó Terrane in the present and previous studies.

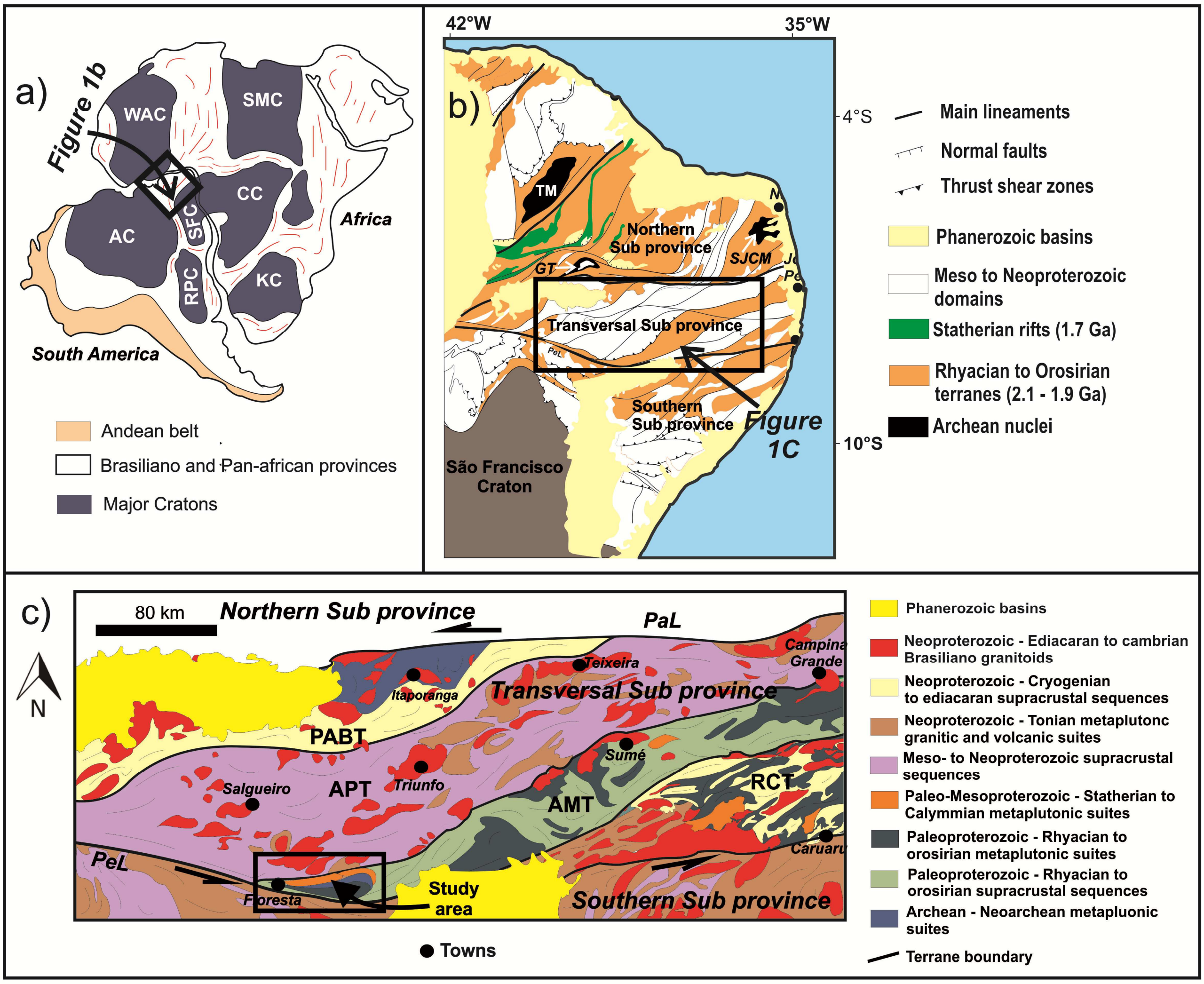


1102

1103 Fig. 1

1104 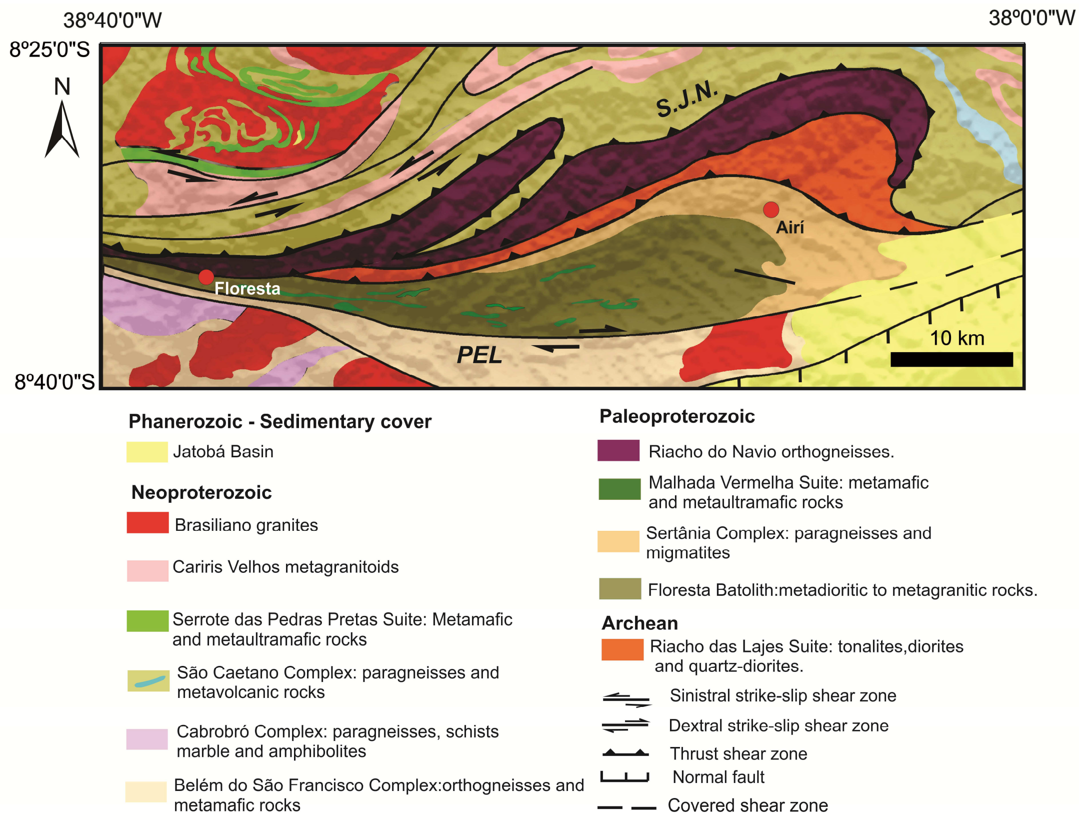


1105 Fig. 2

1106 


1107 Fig. 3

1108 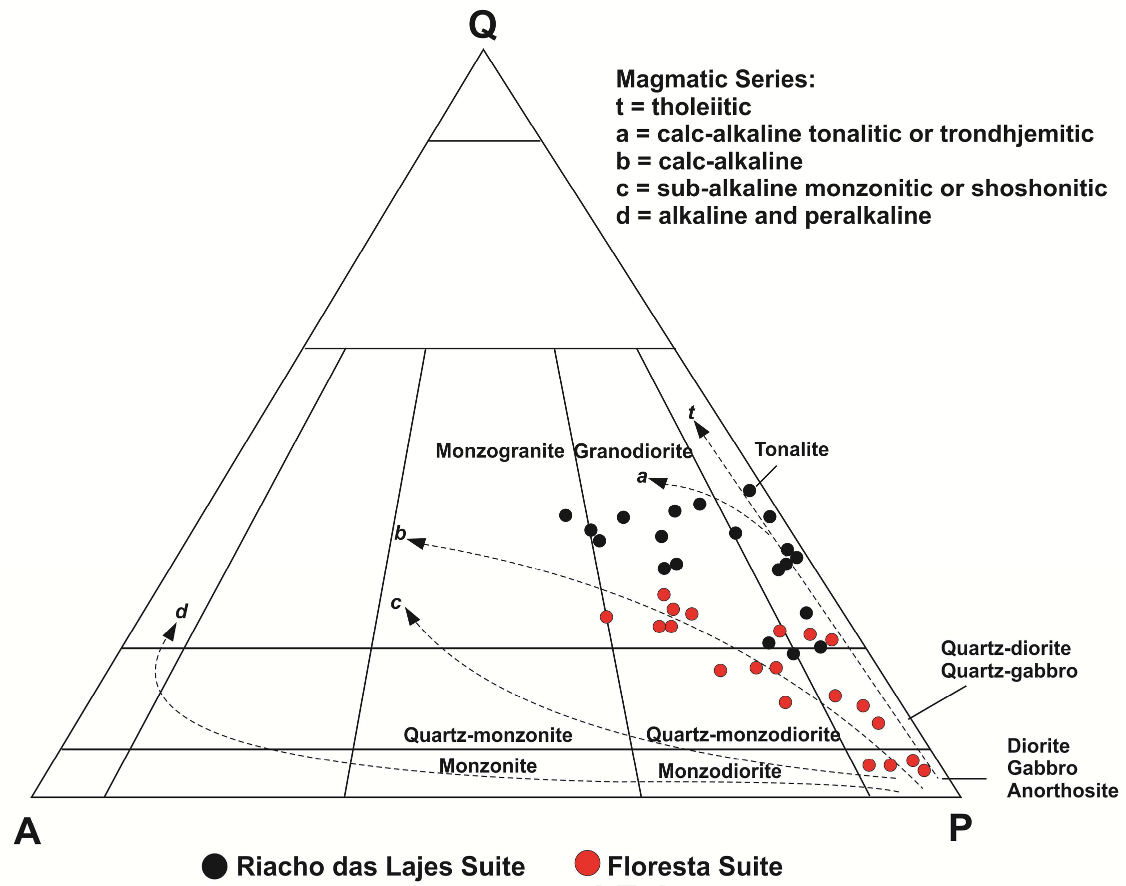


1109 Fig. 4

1110 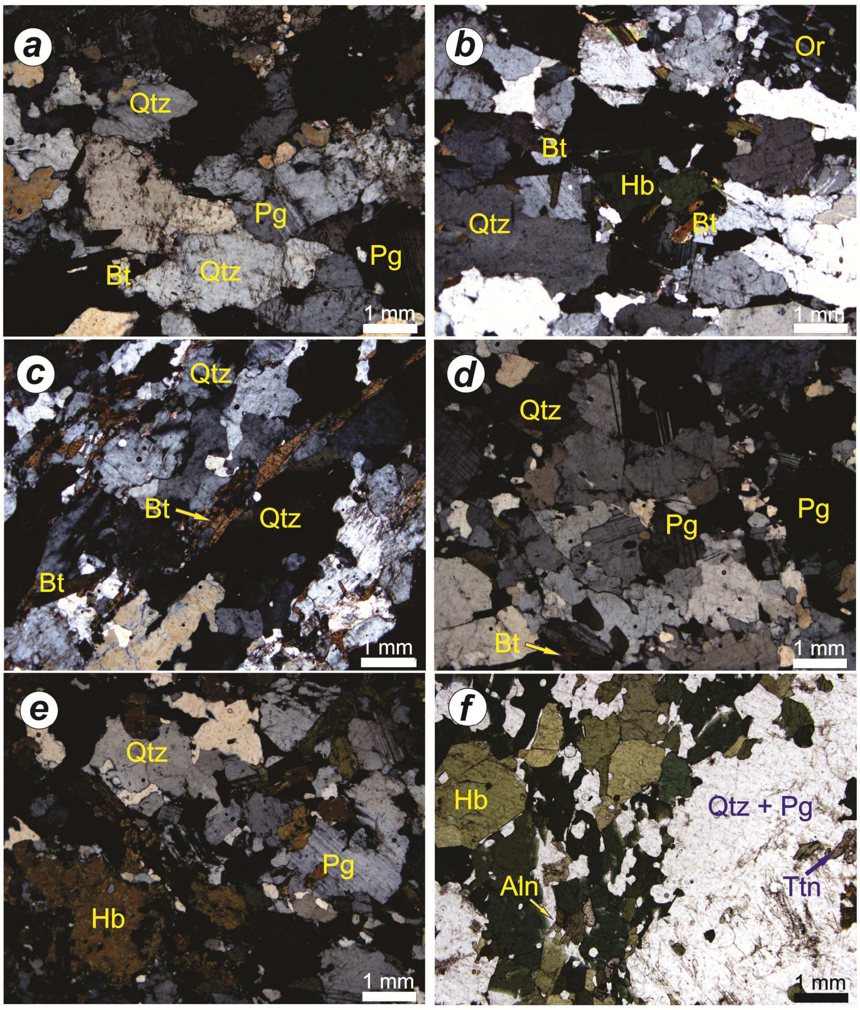


1111 Fig. 5

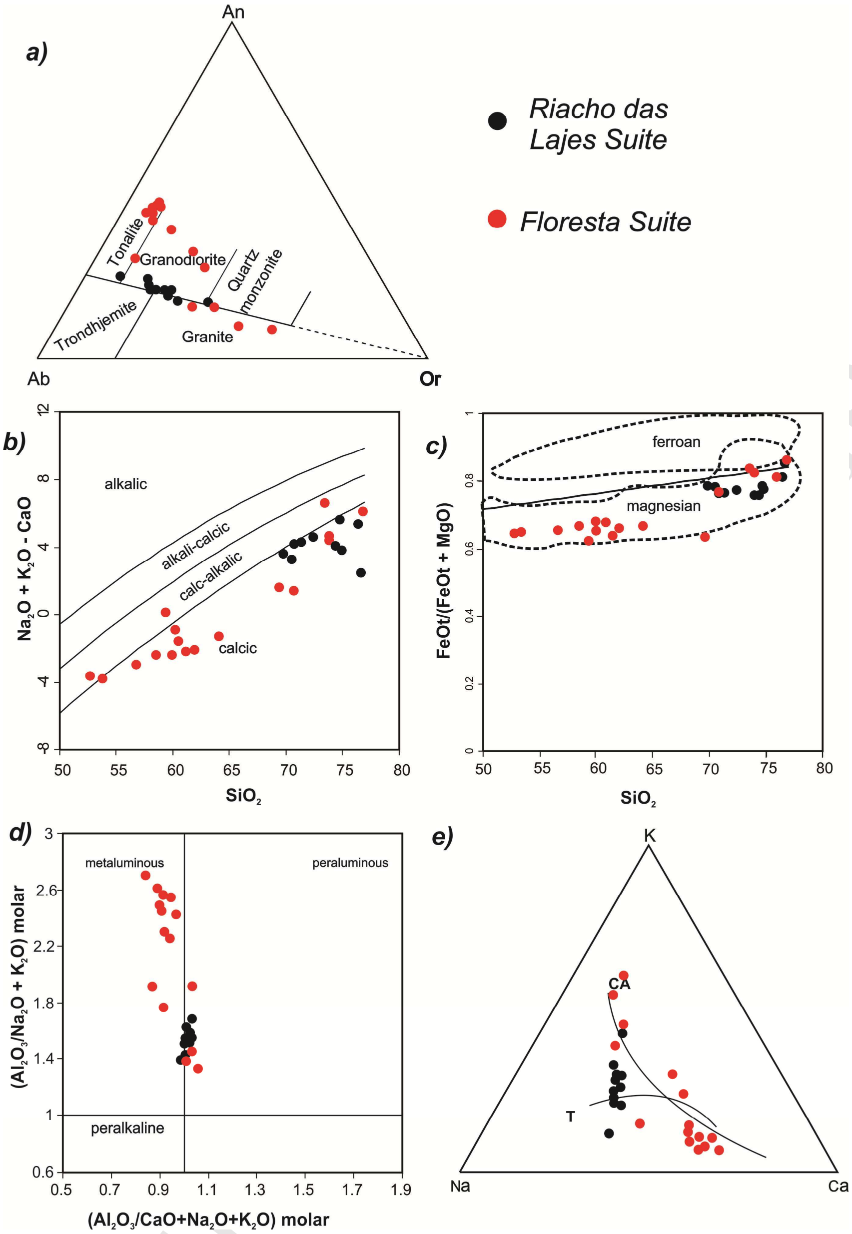


1112

1113 Fig. 6

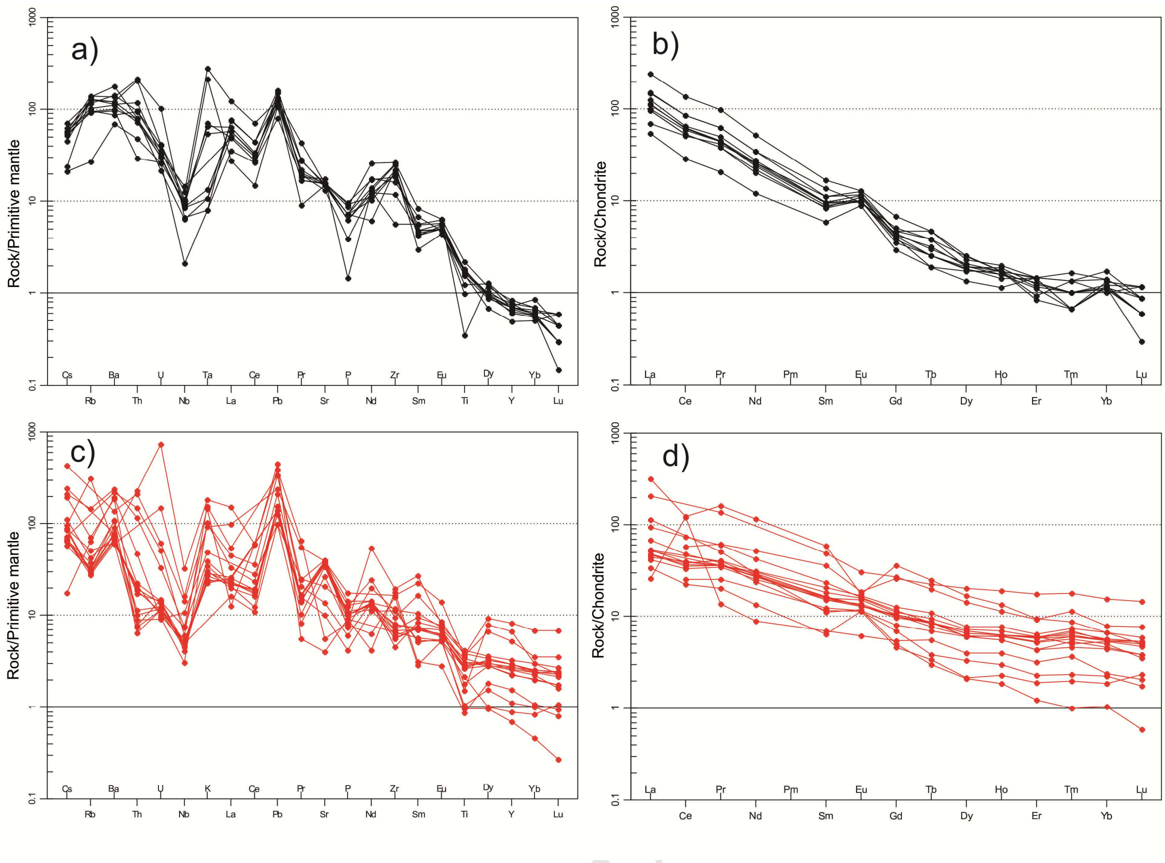


1114

1115 Fig. 7

1116 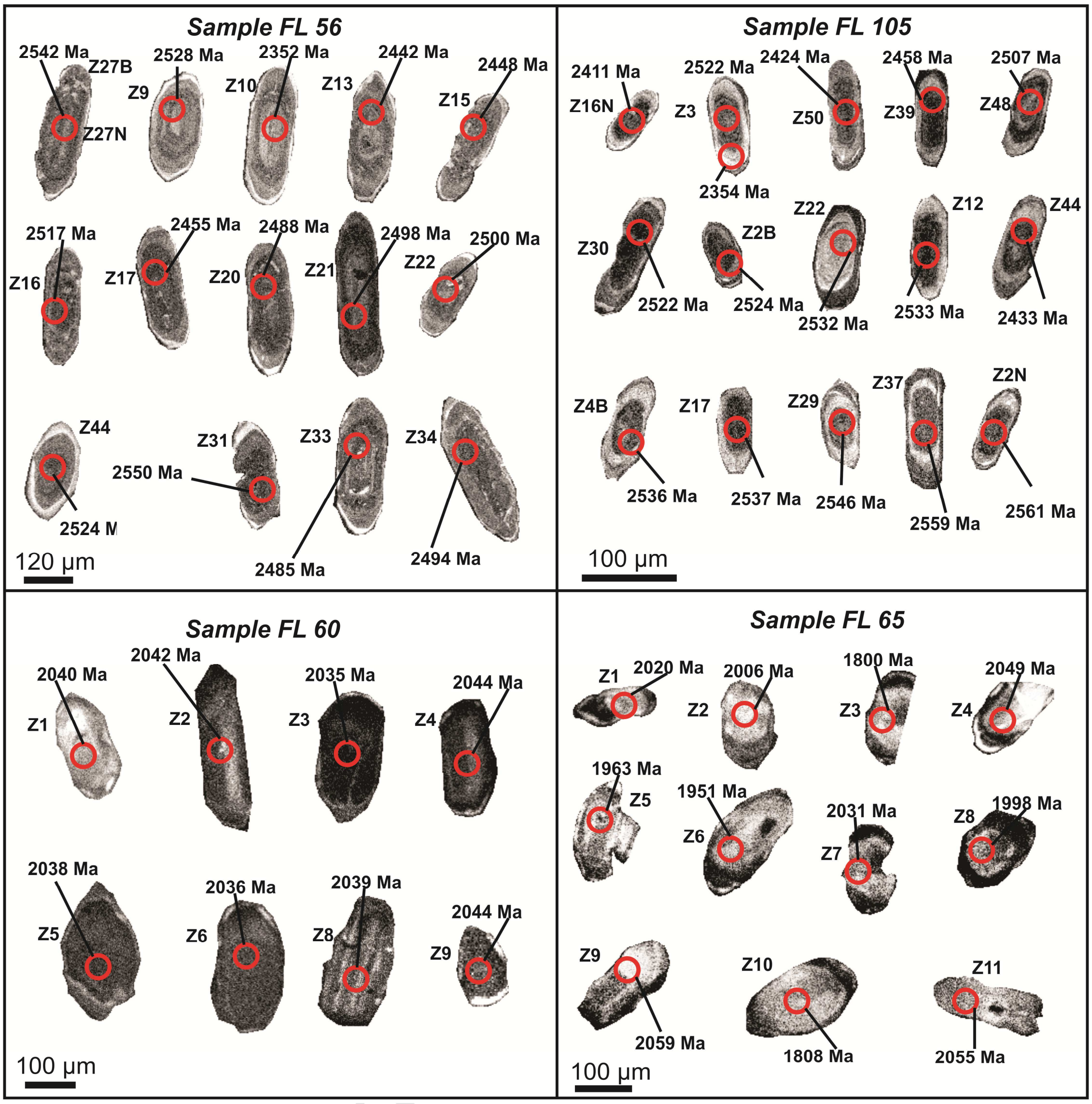


1117 Fig. 8

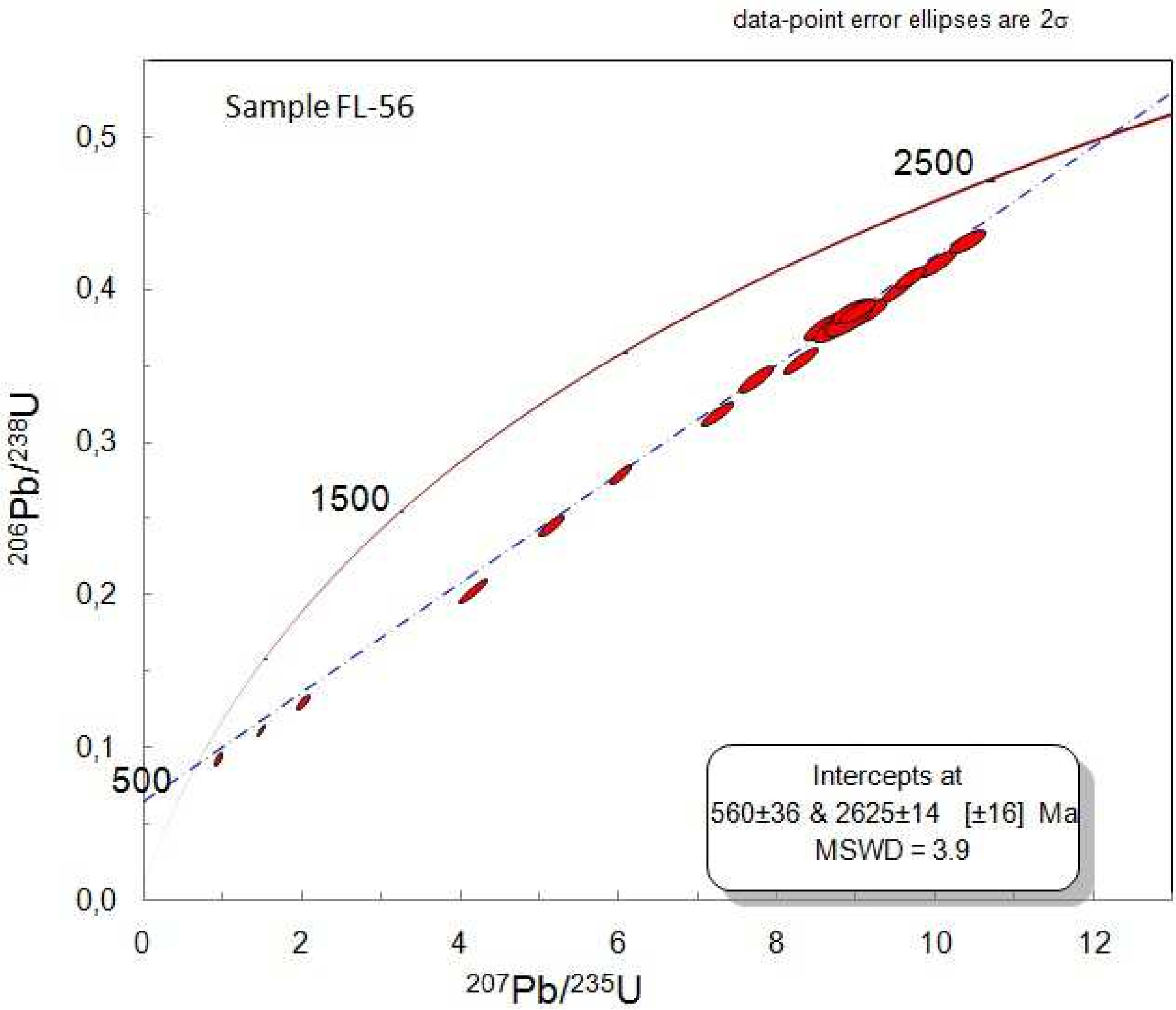


1118

1119 Fig. 9

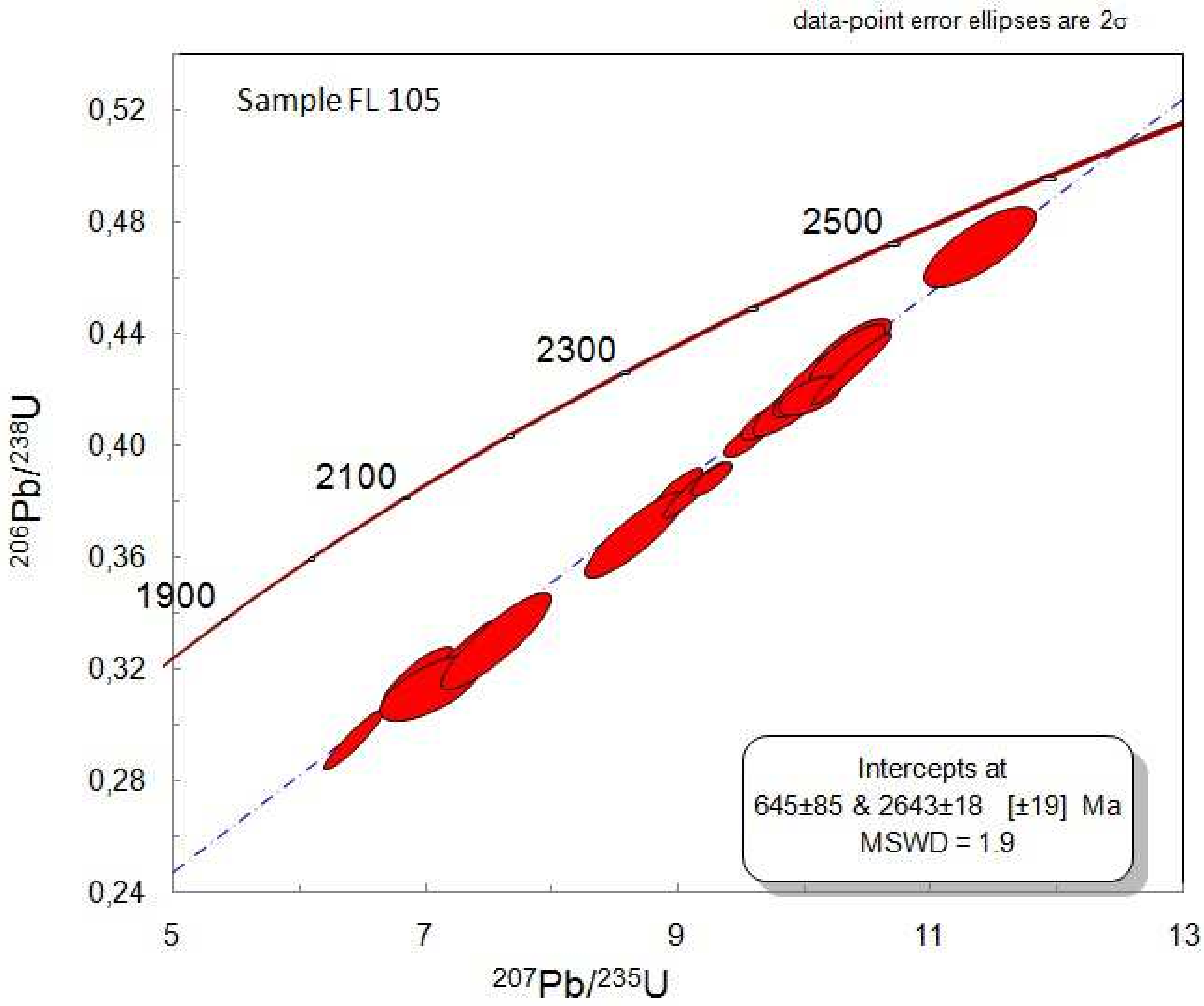


1120

1121 Fig. 10

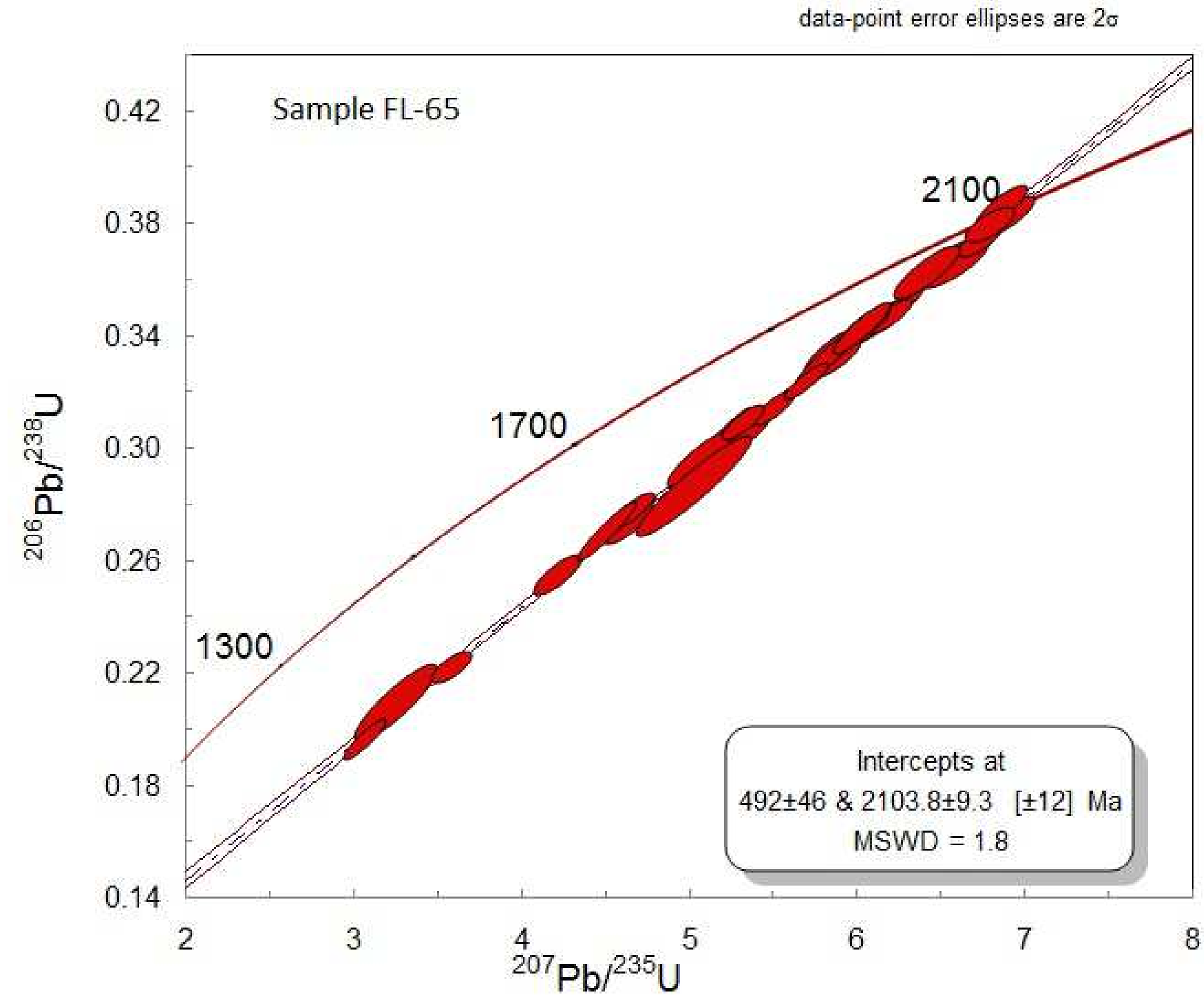
data-point error ellipses are 2σ
Sample FL-65
0.42
0.38
0.34
0.30
0.26
0.22
0.18
0.14
206Pb/238U
2100
1700
1300
Intercepts at
492±46 & 2103.8±9.3 [±12] Ma
MSWD = 1.8
2
3
4
5
6
7
8
207Pb/235U

Fig. 11

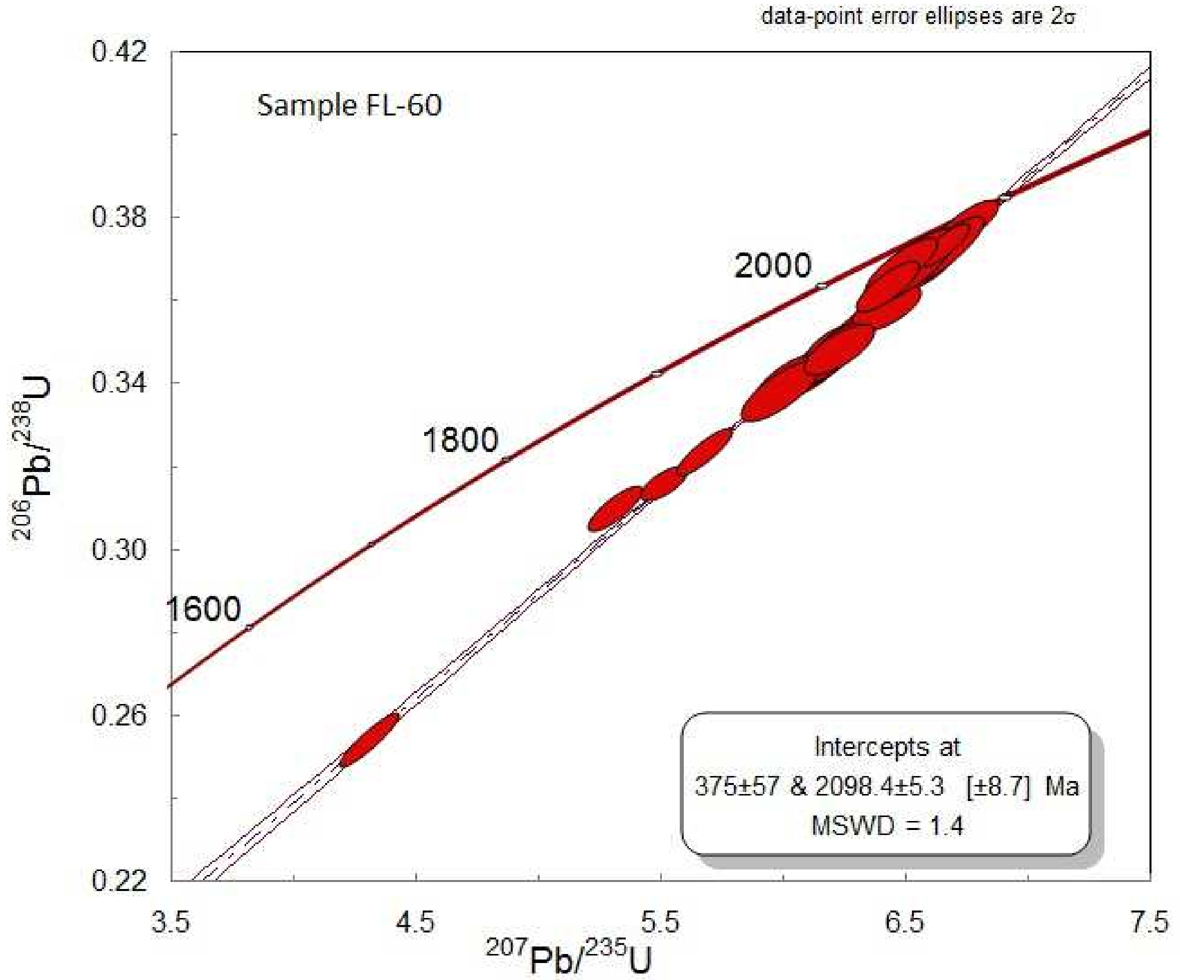


1124

1125 Fig. 12

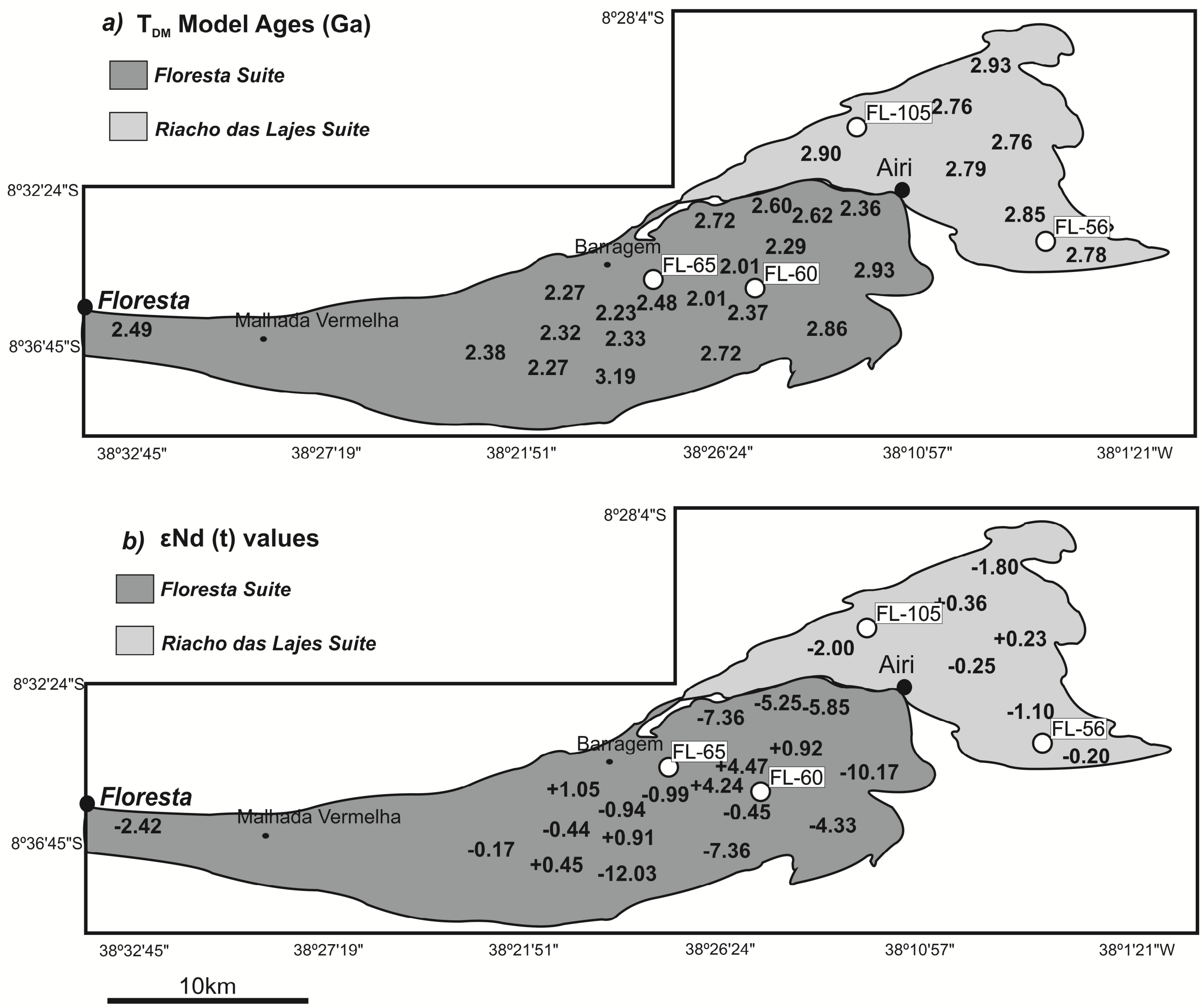
a) T<sub>DM</sub> Model Ages (Ga)
Floresta Suite
Riacho das Lajes Suite
8º28'4"S
8º32'24"S
8º36'45"S
Floresta
Malhada Vermelha
Barragem
Airi
FL-105
FL-56
FL-65
FL-60
2.93
2.76
2.90
2.76
2.79
2.85
2.78
2.72
2.60
2.62
2.36
2.29
2.01
2.93
2.27
2.23
2.48
2.01
2.37
2.86
2.49
2.32
2.33
2.38
2.27
3.19
2.72
38º32'45"
38º27'19"
38º21'51"
38º26'24"
38º10'57"
38º1'21"W
b) εNd (t) values
Floresta Suite
Riacho das Lajes Suite
8º28'4"S
8º32'24"S
8º36'45"S
Floresta
Malhada Vermelha
Barragem
Airi
FL-105
FL-56
FL-65
FL-60
-1.80
+0.36
+0.23
-2.00
-0.25
-1.10
-0.20
-7.36
-5.25
-5.85
+0.92
+4.47
-10.17
+1.05
-0.99
+4.24
-0.94
-0.45
-2.42
-0.44
+0.91
-4.33
-0.17
+0.45
-12.03
-7.36
38º32'45"
38º27'19"
38º21'51"
38º26'24"
38º10'57"
38º1'21"W
10km

Fig. 13

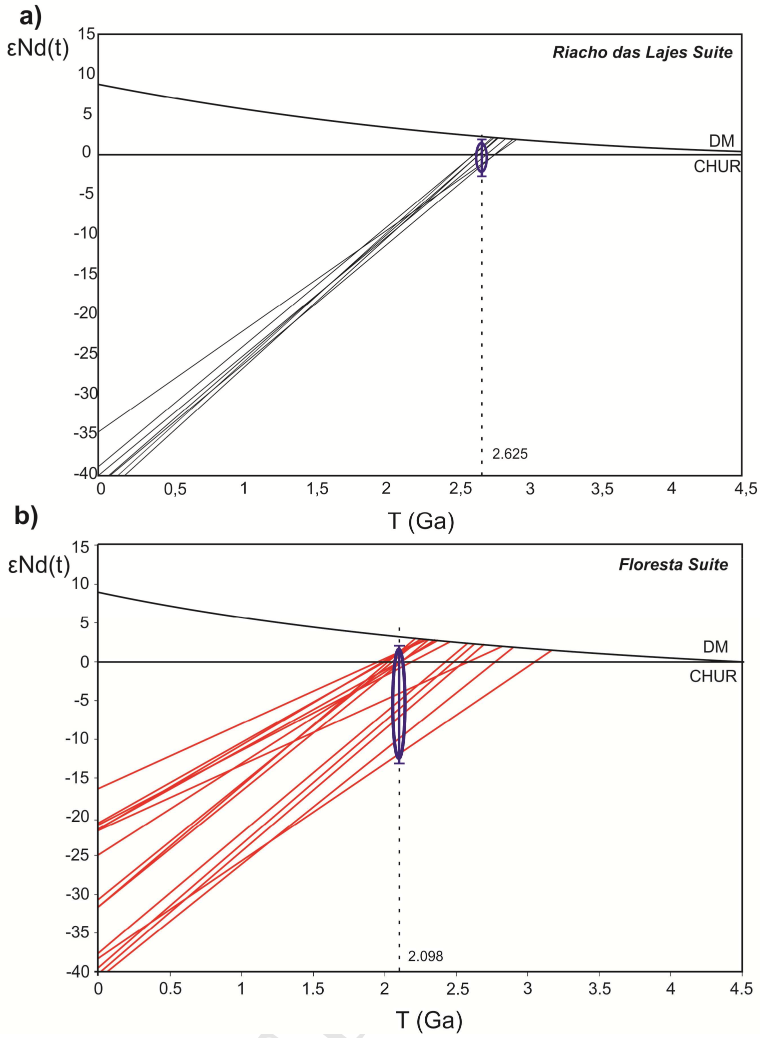


1128

1129 Fig. 14

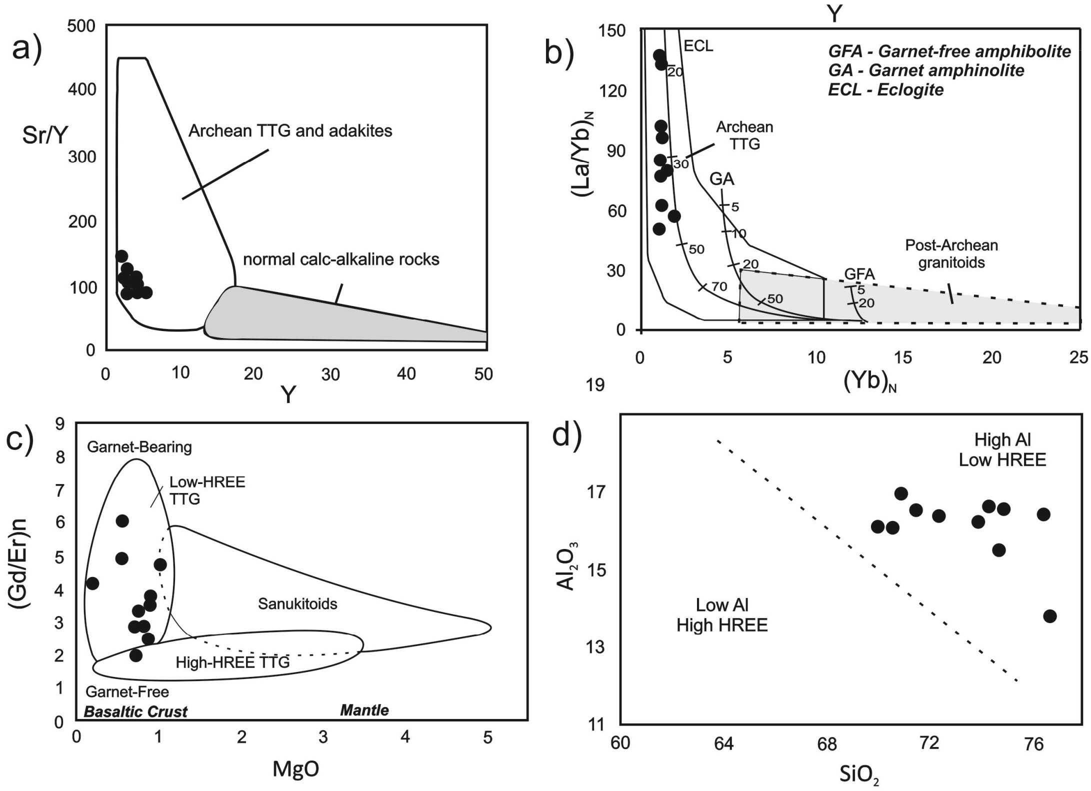


1130

1131 Fig. 15

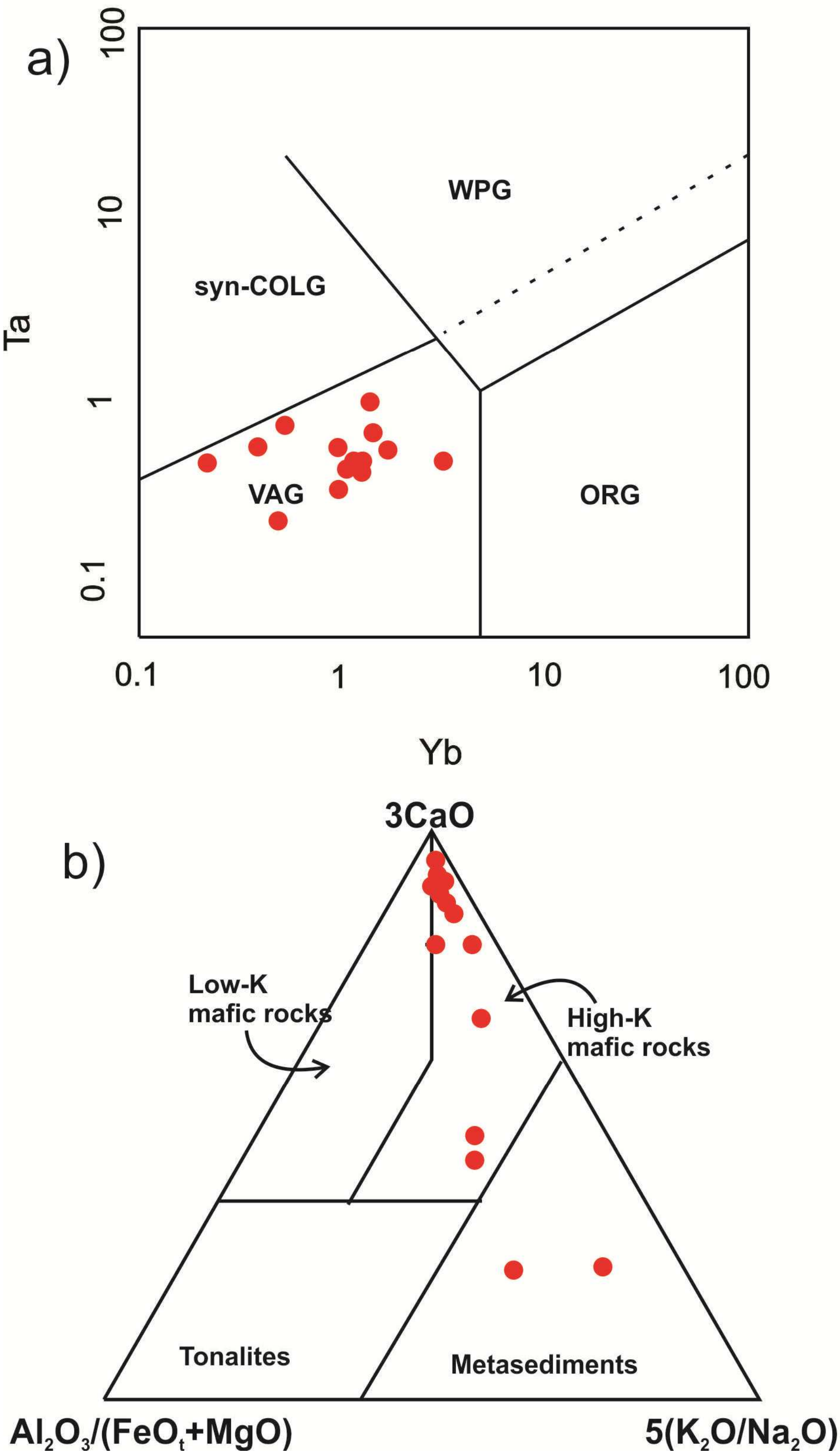


1132

1133 Fig. 16

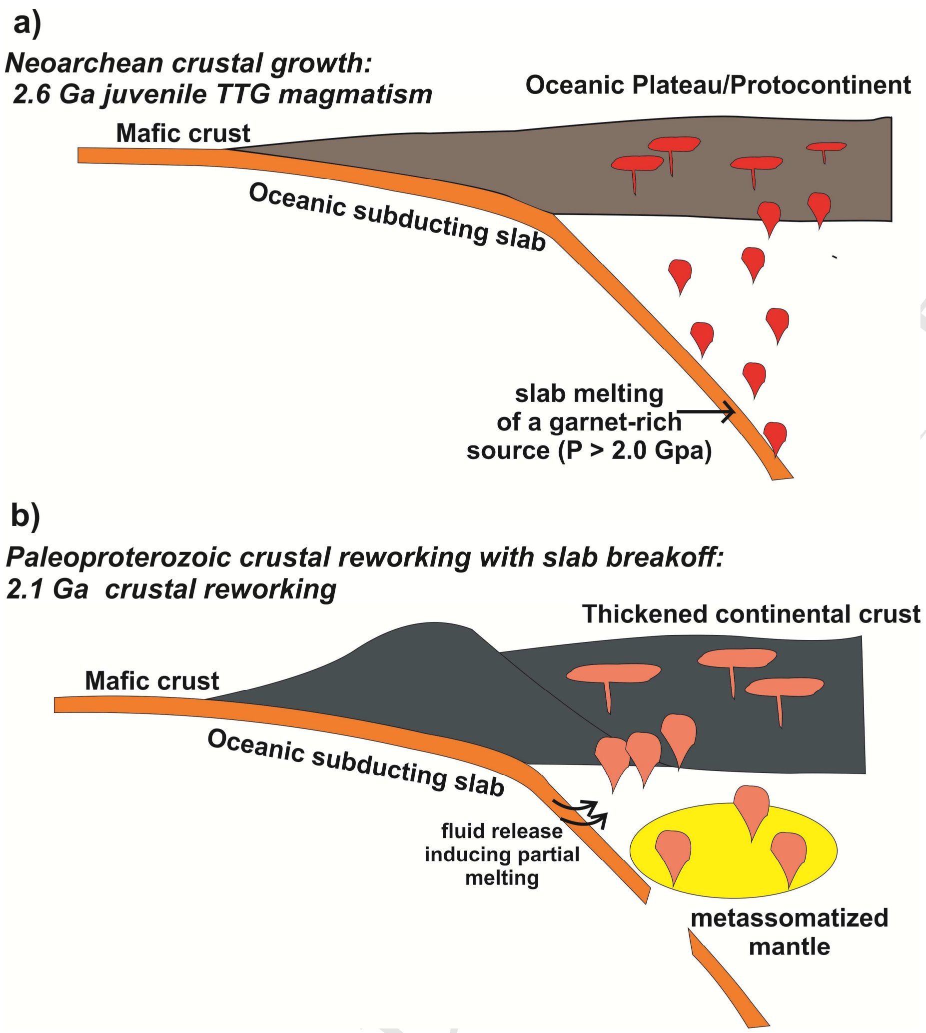


1134

1135 Fig. 17

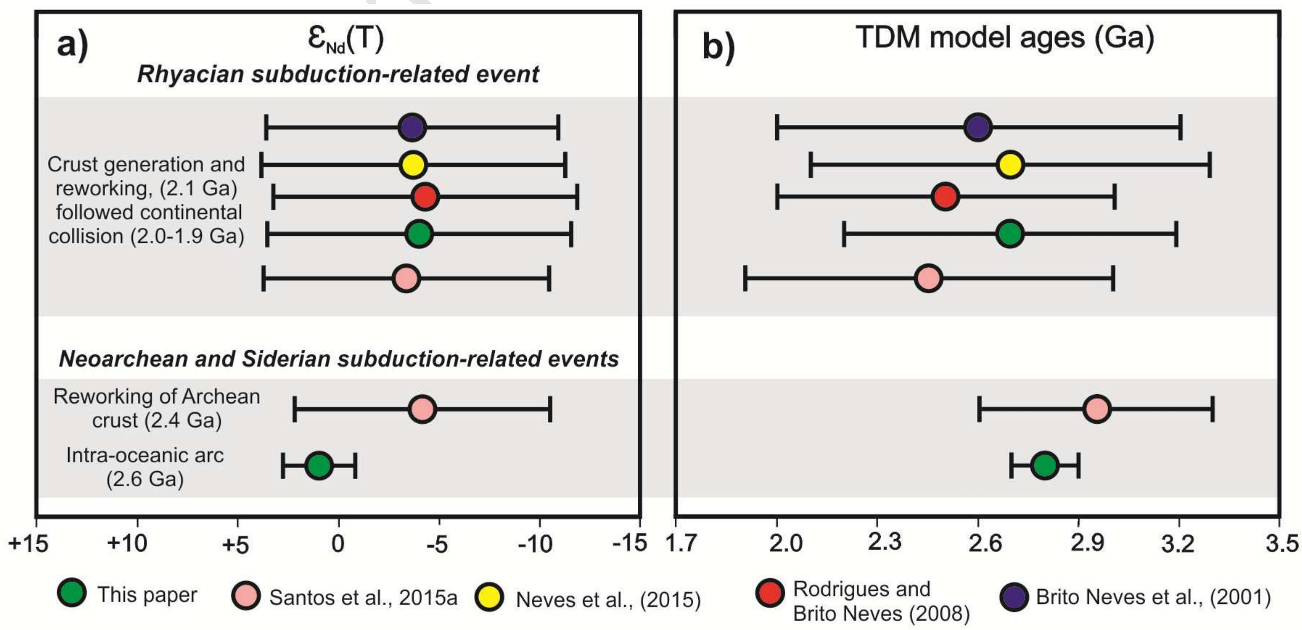


1136

1137 Fig. 18

| Sample | RL 01 | RL 02 | RL 03 | RL 04 | RL 05 | RL 06 | FL 55 | FL 56 | FL 57 | FL 58 | FL 105 |
|---|---|---|---|---|---|---|---|---|---|---|---|
| Major elements (wt.%) | | | | | | | | | | | |
| $Al_2O_3$ | 16.9 | 16.3 | 16.6 | 16.5 | 16.0 | 16.0 | 13.8 | 16.5 | 15.45 | 16.4 | 16.1 |
| CaO | 3.22 | 2.95 | 3.17 | 3.3 | 3.39 | 3.16 | 2.86 | 3.09 | 2.54 | 2.75 | 3.07 |
| $Fe_2O_3$ | 3.69 | 3.20 | 2.8 | 2.78 | 3.11 | 2.97 | 1.04 | 3.16 | 2.12 | 2.64 | 2.98 |
| $Cr_2O_3$ | 0.02 | 0.02 | 0.02 | 0.02 | 0.01 | 0.02 | 0.01 | 0.01 | 0.01 | 0.01 | 0.01 |
| $K_2O$ | 2.69 | 2.89 | 2.36 | 2.17 | 1.88 | 2.05 | 0.83 | 2.75 | 4.23 | 3.35 | 2.87 |
| MgO | 1.02 | 0.84 | 0.8 | 0.71 | 0.78 | 0.73 | 0.15 | 0.88 | 0.53 | 0.54 | 0.86 |
| MnO | 0.04 | 0.03 | 0.03 | 0.03 | 0.03 | 0.03 | 0.02 | 0.03 | 0.02 | 0.03 | 0.03 |
| $Na_2O$ | 4.85 | 4.67 | 5.0 | 5.07 | 4.76 | 4.82 | 4.43 | 4.76 | 3.98 | 4.79 | 4.61 |
| $P_2O_5$ | 0.18 | 0.15 | 0.15 | 0.19 | 0.13 | 0.15 | 0.03 | 0.23 | 0.08 | 0.15 | 0.13 |
| $SiO_2$ | 70.8 | 72.4 | 74.3 | 74.8 | 70.5 | 69.8 | 76.7 | 71.3 | 74.7 | 76.4 | 73.9 |
| $TiO_2$ | 0.44 | 0.37 | 0.34 | 0.31 | 0.35 | 0.32 | 0.07 | 0.35 | 0.2 | 0.25 | 0.34 |
| Trace elements (ppm) | | | | | | | | | | | |
| Ba | 802 | 946 | 733 | 659 | 570 | 631 | 460 | 746 | 1190 | 911 | 796 |
| Ce | 118 | 56.4 | 46.4 | 46.5 | 54.3 | 25.1 | 44.1 | 74.2 | 51.1 | 73.6 | 53.5 |
| Cr | 140 | 150 | 160 | 160 | 110 | 140 | 70.0 | 70.0 | 60.0 | 60.0 | 70.0 |
| Cs | 1.49 | 1.33 | 1.21 | 1.09 | 1.22 | 1.13 | 0.44 | 0.94 | 0.5 | 1.21 | 1.14 |
| Dy | 0.78 | 0.63 | 0.66 | 0.59 | 0.67 | 0.46 | 0.87 | 0.67 | 0.71 | 0.85 | 0.61 |
| Er | 0.33 | 0.32 | 0.28 | 0.32 | 0.33 | 0.33 | 0.26 | 0.29 | 0.21 | 0.19 | 0.25 |
| Eu | 0.99 | 0.78 | 0.84 | 0.77 | 0.87 | 0.68 | 0.97 | 0.89 | 0.75 | 0.74 | 0.77 |
| Ga | 20.4 | 19.8 | 20.2 | 19.8 | 20.3 | 20.7 | 12.0 | 19.7 | 16.9 | 17.4 | 18.8 |
| Gd | 1.89 | 0.98 | 1.16 | 1.11 | 1.17 | 0.81 | 1.3 | 1.31 | 1.23 | 1.4 | 1.06 |
| Hf | 6.9 | 6.7 | 5.3 | 5.7 | 6.3 | 5.6 | 1.8 | 4.8 | 3.2 | 4.4 | 5.2 |
| Ho | 0.14 | 0.1 | 0.13 | 0.12 | 0.12 | 0.08 | 0.12 | 0.11 | 0.12 | 0.12 | 0.11 |
| La | 80.1 | 41.4 | 31.9 | 32.0 | 37.1 | 18.0 | 22.8 | 49.1 | 33.2 | 50.1 | 37.7 |
| Lu | 0.03 | 0.04 | 0.04 | 0.02 | 0.03 | 0.04 | 0.01 | 0.02 | 0.03 | 0.03 | 0.02 |
| Nb | 8.4 | 6.9 | 6.0 | 9.6 | 6.5 | 6.4 | 1.4 | 5.6 | 4.2 | 4.4 | 5.8 |

| | | | | | | | | | | | |
|---|---|---|---|---|---|---|---|---|---|---|---|
| Nd | 32.6 | 17.4 | 12.8 | 14.0 | 16.3 | 7.7 | 16.2 | 21.6 | 15.6 | 22.0 | 15.1 |
| Pr | 11.0 | 5.63 | 4.3 | 4.28 | 5.11 | 2.31 | 4.65 | 6.99 | 4.95 | 7.09 | 4.91 |
| Rb | 75.1 | 69.9 | 61.9 | 56.7 | 58.5 | 56.0 | 16.1 | 77.9 | 82.8 | 84.0 | 76.6 |
| Sm | 3.44 | 1.97 | 1.73 | 1.71 | 1.95 | 1.21 | 2.28 | 2.26 | 1.94 | 2.77 | 1.82 |
| Sn | 1.00 | 1.00 | 1.00 | 1.00 | 1.00 | n.d. | n.d | 1.00 | n.d. | 1.00 | n.d |
| Sr | 311 | 304 | 312 | 316 | 311 | 296 | 352 | 308 | 263 | 294 | 295 |
| Ta | 10.4 | 2.41 | 2.60 | 2.12 | 2.03 | 8.00 | 0.38 | 0.48 | 0.46 | 0.39 | 0.50 |
| Tb | 0.22 | 0.12 | 0.12 | 0.09 | 0.15 | 0.09 | 0.22 | 0.18 | 0.14 | 0.18 | 0.12 |
| Th | 16.6 | 7.73 | 5.74 | 6.25 | 7.63 | 2.35 | 3.87 | 9.55 | 6.36 | 17.25 | 6.34 |
| Tm | 0.04 | 0.02 | 0.03 | 0.02 | 0.05 | 0.04 | 0.03 | 0.03 | 0.04 | 0.02 | 0.02 |
| U | 0.83 | 0.82 | 0.61 | 0.66 | 0.72 | 0.53 | 0.52 | 0.62 | 0.43 | 2.07 | 0.62 |
| V | 32.0 | 31.0 | 27.0 | 25.0 | 26.0 | 25.0 | 7.0 | 31.0 | 14.0 | 17.0 | 27.0 |
| W | 12.0 | 9.0 | 11.0 | 10.0 | 8.0 | 8.0 | 3.0 | 3.0 | 3.0 | 5.0 | 3.0 |
| Y | 3.6 | 3.0 | 3.0 | 3.0 | 3.3 | 2.1 | 3.3 | 2.6 | 3.1 | 2.9 | 2.7 |
| Yb | 0.31 | 0.29 | 0.27 | 0.26 | 0.31 | 0.22 | 0.25 | 0.24 | 0.38 | 0.25 | 0.25 |
| Zr | 278.0 | 268.0 | 212.0 | 228.0 | 261.0 | 229.0 | 59.0 | 193.0 | 125.0 | 170.0 | 205.0 |

Table 1 - Major (wt. %) and trace element (ppm) concentrations of the Riacho das Lajes Suite, Alto Moxotó Terrane, NE Brazil.

| Sample | FL02 | FL05 | FL06 | FL07 | FL09 | FL10 | FL19 | FL51B | FL60 | FL65 | FL122 | FL 20 | FL 67 | FL59 | FL10b | FL20 | FL64 |
|---|---|---|---|---|---|---|---|---|---|---|---|---|---|---|---|---|---|
| Major elements (wt.%) | | | | | | | | | | | | | | | | | |
| $Al_2O_3$ | 13.1 | 18.9 | 18.6 | 19.9 | 20.8 | 15.0 | 18.1 | 15.7 | 17.1 | 18.5 | 13.0 | 13.5 | 16.9 | 14.9 | 17.2 | 17.1 | 18.1 |
| CaO | 1.94 | 7.52 | 7.41 | 8.17 | 8.83 | 3.76 | 6.79 | 2.35 | 6.39 | 6.61 | 1.15 | 1.32 | 6.04 | 4.51 | 6.56 | 6.53 | 8.46 |
| $Fe_2O_3$ | 2.43 | 7.63 | 7.8 | 8.41 | 10.7 | 3.96 | 7.98 | 1.99 | 7.49 | 7.10 | 1.62 | 3.07 | 7.89 | 3.36 | 6.59 | 5.95 | 9.49 |
| $K_2O$ | 3.12 | 0.89 | 0.87 | 0.92 | 1.18 | 1.00 | 1.04 | 4.63 | 2.79 | 0.74 | 4.43 | 5.49 | 1.49 | 3.02 | 0.71 | 0.68 | 0.82 |
| MgO | 0.44 | 3.57 | 3.52 | 4.02 | 5.22 | 1.02 | 3.41 | 0.41 | 4.13 | 3.28 | 0.23 | 0.52 | 3.41 | 1.91 | 3.19 | 3.08 | 4.69 |
| MnO | 0.05 | 0.13 | 0.13 | 0.13 | 0.19 | 0.05 | 0.12 | 0.02 | 0.12 | 0.13 | 0.02 | 0.06 | 0.17 | 0.06 | 0.14 | 0.13 | 0.16 |
| $Na_2O$ | 3.66 | 4.09 | 3.99 | 4.07 | 4.06 | 4.22 | 4.01 | 3.95 | 3.63 | 4.09 | 2.91 | 2.52 | 3.55 | 3.14 | 3.61 | 3.60 | 3.53 |
| $P_2O_5$ | 0.09 | 0.24 | 0.22 | 0.23 | 0.31 | 0.17 | 0.2 | 0.13 | 0.38 | 0.21 | 0.20 | 0.18 | 0.27 | 0.16 | 0.22 | 0.22 | 0.08 |
| $SiO_2$ | 74.4 | 59.8 | 58.4 | 56.4 | 52.5 | 71.1 | 60.4 | 76.2 | 59.2 | 63.8 | 76.71 | 73.50 | 59.9 | 69.5 | 61.4 | 61.3 | 53.1 |
| $TiO_2$ | 0.23 | 0.66 | 0.66 | 0.73 | 0.91 | 0.47 | 0.57 | 0.21 | 0.78 | 0.63 | 0.19 | 0.33 | 0.80 | 0.39 | 0.60 | 0.58 | 0.84 |
| Trace elements (ppm) | | | | | | | | | | | | | | | | | |
| Ba | 1345 | 460 | 473 | 432 | 507 | 746 | 427 | 1545 | 948 | 545 | 418 | 546 | 1290 | 1660 | 641 | 763 | 542 |
| Ce | 41.3 | 31.6 | 34 | 28.7 | 33.3 | 19.4 | 21.8 | 59 | 125 | 30.3 | 104.5 | 106.5 | 49.8 | 63.8 | 34.0 | 33.7 | 34.6 |
| Cr | 60 | 80 | 80 | 70 | 70 | 100 | 130 | 60 | 110 | 60 | n.d. | 10 | 40 | 30 | 20 | 20 | 40 |
| Cs | 0.14 | 0.68 | 0.71 | 0.53 | 0.89 | 0.53 | 0.71 | 0.57 | 3.39 | 0.54 | 0.77 | 1.93 | 1.53 | 1.66 | 0.51 | 0.46 | 0.52 |
| Dy | 1.15 | 2.26 | 2.08 | 2.13 | 2.66 | 0.74 | 2.07 | 0.72 | 4.88 | 2.23 | 1.36 | 5.75 | 6.91 | 2.07 | 2.38 | 2.39 | 2.48 |
| Er | 0.52 | 1.35 | 1.21 | 1.18 | 1.44 | 0.43 | 0.98 | 0.28 | 2.1 | 1.29 | 0.72 | 2.13 | 3.91 | 0.98 | 1.31 | 1.33 | 1.35 |

| | | | | | | | | | | | | | | | | | |
|---|---|---|---|---|---|---|---|---|---|---|---|---|---|---|---|---|---|
| Eu | 0.87 | 1.05 | 1.16 | 1.02 | 1.30 | 0.87 | 0.89 | 0.91 | 2.37 | 0.99 | 0.47 | 1.36 | 1.43 | 1.25 | 1.01 | 1.01 | 1.21 |
| Ga | 11.7 | 17.8 | 18.2 | 18.6 | 21.0 | 14.2 | 18.5 | 17.0 | 19.6 | 18 | 23.5 | 21.3 | 22.1 | 16.2 | 21.9 | 20.8 | 24.7 |
| Gd | 1.92 | 2.8 | 2.87 | 2.84 | 3.47 | 1.27 | 2.24 | 1.38 | 7.53 | 2.89 | 1.50 | 9.93 | 7.21 | 3.24 | 2.81 | 2.69 | 3.09 |
| Hf | 3.4 | 2.0 | 1.6 | 1.6 | 1.9 | 4.4 | 1.9 | 3.3 | 4.8 | 2.3 | 6.2 | 6.4 | 2.9 | 3.4 | 2.3 | 1.8 | 1.5 |
| Ho | 0.21 | 0.44 | 0.43 | 0.42 | 0.54 | 0.16 | 0.39 | 0.13 | 0.80 | 0.44 | 0.28 | 0.95 | 1.33 | 0.39 | 0.44 | 0.44 | 0.49 |
| La | 22.7 | 15.6 | 17.7 | 13.6 | 15.7 | 11.2 | 10.0 | 37.5 | 68.4 | 15.8 | 8.6 | 104.5 | 21.0 | 31.1 | 17.1 | 17.5 | 14.7 |
| Lu | 0.06 | 0.16 | 0.18 | 0.12 | 0.17 | 0.08 | 0.13 | 0.02 | 0.26 | 0.18 | 0.07 | 0.20 | 0.50 | 0.13 | 0.18 | 0.17 | 0.17 |
| Nb | 2.2 | 3.2 | 3.2 | 2.9 | 5.3 | 3.5 | 3.5 | 4.3 | 10.1 | 3.5 | 11.5 | 23.1 | 7.7 | 5.4 | 3.8 | 3.5 | 3.5 |
| Nd | 15.1 | 17.1 | 17.7 | 15.9 | 19.5 | 8.5 | 12.0 | 18.4 | 56.0 | 17.4 | 5.6 | 73.4 | 32.8 | 26.9 | 18.3 | 18.4 | 19.2 |
| Pr | 4.33 | 4.01 | 4.47 | 3.85 | 4.61 | 2.28 | 2.83 | 5.77 | 15.35 | 4.04 | 1.53 | 18.15 | 6.85 | 6.7 | 4.04 | 4.06 | 4.03 |
| Rb | 40.4 | 18.4 | 19.2 | 17.6 | 27.1 | 23.6 | 32.2 | 99.0 | 112.0 | 20.3 | 197.5 | 267.0 | 44.9 | 91.6 | 21.1 | 19.9 | 19.1 |
| Sm | 2.37 | 3.09 | 3.24 | 3.24 | 4.18 | 1.29 | 2.50 | 2.25 | 10.05 | 3.11 | 1.40 | 11.95 | 7.35 | 4.71 | 3.32 | 3.28 | 3.71 |
| Sn | 1 | 1 | 1 | 1 | 1 | n.d. | 1 | n.d. | 2 | 1 | 2 | 4 | 2 | 1 | 1 | 1 | 1 |
| Sr | 213 | 775 | 795 | 841 | 833 | 555 | 721 | 290 | 828 | 768 | 96.1 | 119 | 435 | 834 | 747 | 740 | 745 |
| Ta | 0.21 | 0.40 | 0.45 | 0.33 | 0.61 | 0.52 | 0.52 | 0.44 | 0.51 | 0.43 | 0.78 | 0.91 | 0.49 | 1.02 | 0.45 | 0.42 | 0.48 |
| Tb | 0.18 | 0.4 | 0.41 | 0.36 | 0.51 | 0.16 | 0.33 | 0.14 | 0.93 | 0.40 | 0.26 | 1.18 | 1.05 | 0.40 | 0.39 | 0.40 | 0.45 |
| Th | 4.01 | 1.59 | 1.66 | 0.65 | 1.46 | 1.89 | 1.78 | 12.75 | 17.9 | 0.86 | 80.0 | 19.35 | 0.76 | 9.88 | 0.54 | 0.63 | 0.97 |
| Tm | 0.07 | 0.15 | 0.18 | 0.17 | 0.22 | 0.06 | 0.16 | 0.0.03 | 0.34 | 0.18 | 0.11 | 0.26 | 0.54 | 0.14 | 0.20 | 0.21 | 0.19 |
| U | 0.2 | 0.23 | 0.29 | 0.31 | 0.3 | 0.3 | 0.21 | 1.07 | 1.29 | 0.25 | 3.15 | 16.35 | 0.19 | 0.70 | 0.24 | 0.25 | 0.26 |

| | | | | | | | | | | | | | | | | | |
|---|---|---|---|---|---|---|---|---|---|---|---|---|---|---|---|---|---|
| V | 21 | 160 | 167 | 174 | 217 | 47 | 163 | 13 | 168 | 153 | 13 | 19 | 138 | 77 | 138 | 129 | 211 |
| W | 4 | 4 | 3 | 7 | 2 | 5 | 3 | 3 | 3 | 2 | 76 | 14 | 49 | 37 | 97 | 11 | 5 |
| Y | 5.1 | 11.9 | 12.3 | 11 | 14.7 | 4.1 | 10.3 | 3.2 | 23.7 | 12.6 | 7.1 | 30.6 | 37.4 | 10.5 | 13.5 | 13.5 | 13.5 |
| Yb | 0.5 | 1.17 | 1.26 | 1.11 | 1.48 | 0.41 | 1.01 | 0.23 | 1.74 | 1.19 | 0.53 | 1.47 | 3.38 | 0.98 | 1.25 | 1.21 | 1.20 |
| Zr | 126 | 77 | 62 | 63 | 78 | 178 | 74 | 132 | 183 | 91 | 199 | 220 | 107 | 128 | 86 | 67 | 51 |

Table 2 - Major (wt. %) and trace element (ppm) concentrations of the Floresta Suite, Alto Moxotó Terrane, NE Brazil. n.d. = not detected.

| Grain spot | **Isotopic ratios** $^{207}Pb/^{206}Pb$ | ± (1σ) | $^{207}Pb/^{235}U$ | ± (1σ) | $^{206}Pb/^{238}U$ | ± (1σ) | **Ages** $^{207}Pb/^{206}Pb$ | ± (1σ) | $^{207}Pb/^{235}U$ | ± (1σ) | $^{206}Pb/^{238}U$ | ± (1σ) | Rho | Th/U | Conc. (%) |
|---|---|---|---|---|---|---|---|---|---|---|---|---|---|---|---|
| Z7N | 0.17 | 0.51 | 10.05 | 0.95 | 0.42 | 0.81 | 2541.90 | 8.84 | 2439.75 | 8.81 | 2264.08 | 15.37 | 0.82 | 0.34 | 92.80 |
| Z7B | 0.17 | 0.42 | 9.58 | 0.97 | 0.40 | 0.88 | 2528.10 | 7.29 | 2394.90 | 8.96 | 2187.97 | 16.29 | 0.89 | 0.28 | 91.36 |
| Z8 | 0.11 | 0.95 | 2.15 | 1.65 | 0.14 | 1.35 | 1759.20 | 17.32 | 1163.78 | 11.36 | 847.93 | 10.69 | 0.82 | 0.30 | 72.86 |
| Z9 | 0.15 | 0.55 | 5.24 | 1.13 | 0.25 | 0.98 | 2301.07 | 9.67 | 1859.24 | 9.60 | 1452.83 | 12.80 | 0.86 | 0.46 | 78.14 |
| Z10 | 0.15 | 0.43 | 6.10 | 0.88 | 0.29 | 0.77 | 2351.98 | 7.60 | 1990.24 | 7.72 | 1619.64 | 11.06 | 0.85 | 0.14 | 81.38 |
| Z13 | 0.16 | 0.54 | 7.80 | 1.08 | 0.35 | 0.94 | 2441.53 | 9.42 | 2208.00 | 9.76 | 1917.48 | 15.60 | 0.85 | 0.10 | 86.84 |
| Z15 | 0.16 | 0.50 | 7.32 | 1.10 | 0.32 | 0.97 | 2448.32 | 8.78 | 2151.18 | 9.79 | 1808.49 | 15.35 | 0.88 | 0.36 | 84.07 |
| Z16 | 0.17 | 0.73 | 9.15 | 1.20 | 0.39 | 0.95 | 2517.25 | 12.70 | 2353.60 | 11.03 | 2117.40 | 17.23 | 0.78 | 0.21 | 89.96 |
| Z17 | 0.16 | 0.58 | 8.61 | 1.06 | 0.38 | 0.89 | 2454.79 | 10.06 | 2297.77 | 9.65 | 2074.25 | 15.76 | 0.82 | 0.21 | 90.27 |
| Z20 | 0.17 | 0.80 | 8.80 | 1.33 | 0.38 | 1.07 | 2487.71 | 13.83 | 2317.30 | 12.16 | 2077.69 | 18.98 | 0.79 | 0.23 | 89.66 |
| Z21 | 0.17 | 0.88 | 8.95 | 1.38 | 0.38 | 1.06 | 2497.68 | 15.29 | 2332.43 | 12.56 | 2096.71 | 18.89 | 0.75 | 0.31 | 89.89 |
| Z22 | 0.17 | 0.46 | 8.35 | 1.05 | 0.36 | 0.94 | 2499.71 | 8.01 | 2269.58 | 9.52 | 1974.08 | 16.02 | 0.89 | 0.26 | 86.98 |
| Z25 | 0.08 | 1.31 | 1.08 | 1.94 | 0.10 | 1.43 | 1021.96 | 26.30 | 743.06 | 10.17 | 636.39 | 8.66 | 0.76 | 0.32 | 85.64 |
| Z31 | 0.17 | 0.52 | 10.43 | 0.84 | 0.43 | 0.66 | 2550.09 | 8.98 | 2473.74 | 7.82 | 2325.60 | 12.98 | 0.75 | 0.40 | 94.01 |
| Z33 | 0.17 | 0.80 | 9.01 | 1.14 | 0.39 | 0.81 | 2485.13 | 13.92 | 2338.84 | 10.44 | 2122.72 | 14.70 | 0.68 | 0.30 | 90.76 |
| Z34 | 0.17 | 0.57 | 9.06 | 0.99 | 0.39 | 0.81 | 2493.80 | 9.91 | 2344.22 | 9.07 | 2124.06 | 14.66 | 0.79 | 0.25 | 90.61 |

Table 3 - Summary of LA-ICP-MS data of zircons from sample LS-56 (Riacho das Lajes Suite).

| | **Isotopic ratios** | | | | | | **Ages** | | | | | | | | |
|---|---|---|---|---|---|---|---|---|---|---|---|---|---|---|---|
| Grain spot | $^{207}Pb/^{206}Pb$ | ± (1σ) | $^{207}Pb/^{235}U$ | ± (1σ) | $^{206}Pb/^{238}U$ | ± (1σ) | $^{207}Pb/^{206}Pb$ | ± (1σ) | $^{207}Pb/^{235}U$ | ± (1σ) | $^{206}Pb/^{238}U$ | ± (1σ) | Rho | Th/U | Conc. (%) |
| Z16 | 0.16 | 0.52 | 6.51 | 1.48 | 0.30 | 1.39 | 2375.27 | 8.77 | 2047.38 | 12.94 | 1694.98 | 20.62 | 0.94 | 0.13 | 82.79 |
| Z52 | 0.16 | 0.92 | 7.00 | 1.67 | 0.32 | 1.39 | 2380.10 | 16.10 | 2110.85 | 14.82 | 1800.48 | 21.88 | 0.83 | 0.05 | 85.30 |
| Z6N | 0.16 | 0.42 | 7.28 | 1.80 | 0.33 | 1.75 | 2414.84 | 7.26 | 2146.17 | 16.05 | 1830.91 | 27.88 | 0.97 | 0.23 | 85.31 |
| Z50 | 0.16 | 1.70 | 7.11 | 2.24 | 0.32 | 1.46 | 2423.83 | 28.53 | 2124.71 | 19.76 | 1784.61 | 22.75 | 0.67 | 0.15 | 83.99 |
| Z39 | 0.16 | 1.12 | 7.62 | 2.33 | 0.34 | 2.04 | 2458.08 | 18.79 | 2187.38 | 20.67 | 1863.86 | 32.94 | 0.88 | 0.23 | 85.21 |
| Z23 | 0.17 | 0.39 | 9.04 | 0.86 | 0.39 | 0.76 | 2497.96 | 6.68 | 2342.34 | 7.83 | 2115.89 | 13.79 | 0.88 | 0.16 | 90.33 |
| Z48 | 0.17 | 0.89 | 8.71 | 1.87 | 0.37 | 1.64 | 2506.76 | 15.48 | 2307.99 | 17.00 | 2039.74 | 28.65 | 0.87 | 0.15 | 88.38 |
| Z3 | 0.17 | 0.36 | 9.16 | 1.07 | 0.39 | 1.01 | 2521.97 | 6.14 | 2354.19 | 9.82 | 2113.50 | 18.23 | 0.94 | 0.28 | 89.78 |
| Z30 | 0.17 | 0.42 | 9.57 | 0.72 | 0.41 | 0.58 | 2522.02 | 7.19 | 2394.53 | 6.59 | 2193.95 | 10.85 | 0.76 | 0.36 | 91.62 |
| Z2B | 0.17 | 0.50 | 9.74 | 0.84 | 0.41 | 0.68 | 2524.31 | 8.72 | 2410.78 | 7.77 | 2224.42 | 12.71 | 0.77 | 0.43 | 92.27 |
| Z22 | 0.17 | 0.39 | 9.31 | 0.73 | 0.39 | 0.62 | 2532.17 | 6.77 | 2368.60 | 6.69 | 2130.94 | 11.17 | 0.80 | 0.35 | 89.97 |
| Z12 | 0.17 | 0.76 | 10.38 | 1.28 | 0.44 | 1.03 | 2532.92 | 13.13 | 2469.69 | 11.86 | 2337.09 | 20.19 | 0.79 | 0.43 | 94.63 |
| Z44 | 0.17 | 0.69 | 9.93 | 1.26 | 0.42 | 1.06 | 2533.00 | 11.96 | 2428.32 | 11.65 | 2250.62 | 20.06 | 0.82 | 0.18 | 92.68 |
| Z4B | 0.17 | 0.78 | 10.18 | 1.56 | 0.43 | 1.36 | 2536.40 | 13.45 | 2451.50 | 14.47 | 2294.81 | 26.19 | 0.86 | 0.27 | 93.61 |
| Z17 | 0.17 | 0.65 | 10.37 | 1.17 | 0.44 | 0.98 | 2537.14 | 11.16 | 2468.35 | 10.87 | 2329.33 | 19.15 | 0.82 | 0.36 | 94.37 |
| Z29 | 0.17 | 0.77 | 10.08 | 1.02 | 0.42 | 0.67 | 2546.49 | 13.35 | 2442.20 | 9.44 | 2263.93 | 12.73 | 0.61 | 0.18 | 92.70 |
| Z37 | 0.18 | 1.01 | 11.41 | 1.58 | 0.47 | 1.22 | 2558.54 | 17.33 | 2556.97 | 14.75 | 2495.37 | 25.20 | 0.76 | 0.29 | 97.59 |
| Z2N | 0.18 | 0.33 | 10.40 | 1.22 | 0.43 | 1.18 | 2560.98 | 5.73 | 2470.86 | 11.33 | 2306.89 | 22.82 | 0.96 | 0.44 | 93.36 |

Table 4 - Summary of LA-ICP-MS data of zircons from sample FL-105 (Riacho das Lajes Suite).

| | **Isotopic ratios** | | | | | | **Ages** | | | | | | | | |
|---|---|---|---|---|---|---|---|---|---|---|---|---|---|---|---|
| Grain spot | $^{207}Pb/^{206}Pb$ | ± (1σ) | $^{207}Pb/^{235}U$ | ± (1σ) | $^{206}Pb/^{238}U$ | ± (1σ) | $^{207}Pb/^{206}Pb$ | ± (1σ) | $^{207}Pb/^{235}U$ | ± (1σ) | $^{206}Pb/^{238}U$ | ± (1σ) | Rho | Th/U | Conc. (%) |
| Z1 | 0.13 | 0.65 | 5.87 | 1.13 | 0.33 | 0.93 | 2019.98 | 11.85 | 1956.81 | 9.83 | 1851.22 | 14.93 | 0.80 | 0.21 | 94.60 |
| Z2 | 0.12 | 0.77 | 4.23 | 1.34 | 0.26 | 1.10 | 1906.44 | 14.16 | 1680.15 | 11.02 | 1467.06 | 14.45 | 0.81 | 0.22 | 87.32 |
| Z3 | 0.11 | 1.39 | 3.28 | 3.01 | 0.21 | 2.67 | 1799.81 | 25.94 | 1475.51 | 23.43 | 1228.33 | 29.91 | 0.89 | 0.23 | 83.25 |
| Z4 | 0.13 | 0.79 | 6.58 | 1.29 | 0.37 | 1.03 | 2049.02 | 14.33 | 2056.16 | 11.40 | 2013.41 | 17.74 | 0.78 | 0.20 | 97.92 |
| Z5 | 0.12 | 0.36 | 5.24 | 1.18 | 0.31 | 1.12 | 1963.47 | 6.66 | 1859.60 | 10.06 | 1724.45 | 16.99 | 0.95 | 0.31 | 92.73 |
| Z6 | 0.12 | 0.78 | 4.65 | 1.35 | 0.27 | 1.09 | 1950.71 | 14.39 | 1758.48 | 11.25 | 1561.26 | 15.18 | 0.80 | 0.28 | 88.78 |
| Z7 | 0.13 | 0.44 | 6.13 | 1.05 | 0.35 | 0.96 | 2031.00 | 7.93 | 1994.29 | 9.19 | 1911.34 | 15.85 | 0.90 | 0.24 | 95.84 |
| Z8 | 0.13 | 0.68 | 5.34 | 1.15 | 0.31 | 0.92 | 1998.47 | 12.48 | 1875.42 | 9.80 | 1722.75 | 13.92 | 0.79 | 0.26 | 91.86 |
| Z9 | 0.13 | 0.46 | 6.90 | 0.89 | 0.38 | 0.76 | 2059.23 | 8.44 | 2099.07 | 7.91 | 2088.51 | 13.58 | 0.83 | 0.30 | 99.50 |
| Z10 | 0.11 | 0.67 | 3.09 | 1.60 | 0.20 | 1.45 | 1807.86 | 12.53 | 1430.81 | 12.28 | 1160.45 | 15.44 | 0.90 | 0.39 | 81.10 |
| Z11 | 0.13 | 0.47 | 6.74 | 0.79 | 0.37 | 0.63 | 2054.71 | 8.61 | 2077.25 | 6.96 | 2049.42 | 11.04 | 0.76 | 0.43 | 98.66 |
| Z12 | 0.12 | 0.60 | 4.67 | 1.20 | 0.28 | 1.04 | 1932.26 | 11.06 | 1761.77 | 10.05 | 1581.14 | 14.60 | 0.86 | 0.20 | 89.75 |
| Z13 | 0.13 | 0.49 | 5.52 | 0.92 | 0.31 | 0.78 | 2007.40 | 8.99 | 1903.16 | 7.91 | 1764.49 | 12.01 | 0.82 | 0.29 | 92.71 |
| Z14 | 0.12 | 0.60 | 5.08 | 0.91 | 0.30 | 0.69 | 1966.13 | 10.93 | 1833.19 | 7.74 | 1675.83 | 10.19 | 0.72 | 0.35 | 91.42 |
| Z15 | 0.13 | 0.57 | 5.86 | 1.15 | 0.33 | 1.00 | 2004.80 | 10.47 | 1955.13 | 10.01 | 1861.92 | 16.21 | 0.86 | 0.32 | 95.23 |
| Z16 | 0.13 | 0.42 | 6.21 | 1.29 | 0.35 | 1.22 | 2037.21 | 7.71 | 2006.12 | 11.26 | 1927.98 | 20.26 | 0.94 | 0.45 | 96.11 |
| Z17 | 0.12 | 0.86 | 3.61 | 1.31 | 0.22 | 0.99 | 1871.08 | 16.02 | 1552.27 | 10.45 | 1295.05 | 11.63 | 0.74 | 0.29 | 83.43 |
| Z18 | 0.13 | 0.43 | 6.20 | 0.84 | 0.35 | 0.72 | 2042.34 | 7.76 | 2005.11 | 7.32 | 1921.24 | 11.97 | 0.84 | 0.24 | 95.82 |
| Z19 | 0.12 | 0.73 | 5.07 | 1.54 | 0.30 | 1.36 | 1962.88 | 13.39 | 1831.81 | 13.06 | 1676.13 | 20.01 | 0.88 | 0.33 | 91.50 |

| | | | | | | | | | | | | | | | |
|---|---|---|---|---|---|---|---|---|---|---|---|---|---|---|---|
| Z21 | 0.13 | 0.44 | 5.82 | 1.28 | 0.33 | 1.20 | 2007.64 | 8.01 | 1949.84 | 11.09 | 1849.49 | 19.33 | 0.94 | 0.23 | 94.85 |
| Z22 | 0.12 | 0.51 | 5.33 | 0.95 | 0.31 | 0.80 | 1977.04 | 9.27 | 1874.46 | 8.10 | 1739.34 | 12.21 | 0.83 | 0.33 | 92.79 |
| Z23 | 0.13 | 0.55 | 6.06 | 0.97 | 0.34 | 0.80 | 2015.97 | 10.01 | 1985.23 | 8.44 | 1908.20 | 13.18 | 0.80 | 0.27 | 96.12 |
| Z24 | 0.13 | 0.63 | 6.42 | 1.23 | 0.36 | 1.06 | 2026.29 | 11.44 | 2035.27 | 10.82 | 1994.67 | 18.18 | 0.85 | 0.36 | 98.00 |
| Z25 | 0.12 | 0.53 | 4.53 | 1.62 | 0.27 | 1.53 | 1921.64 | 9.77 | 1735.95 | 13.45 | 1546.38 | 21.01 | 0.94 | 0.24 | 89.08 |
| Z26 | 0.13 | 0.49 | 6.87 | 0.92 | 0.39 | 0.78 | 2032.35 | 8.89 | 2094.51 | 8.14 | 2106.53 | 13.97 | 0.83 | 0.34 | 100.57 |
| Z27 | 0.13 | 0.57 | 6.80 | 0.88 | 0.38 | 0.66 | 2044.60 | 10.43 | 2085.20 | 7.75 | 2075.39 | 11.73 | 0.71 | 0.40 | 99.53 |
| Z28 | 0.13 | 0.50 | 6.04 | 1.19 | 0.34 | 1.08 | 2013.95 | 9.13 | 1980.94 | 10.40 | 1901.95 | 17.86 | 0.90 | 0.23 | 96.01 |
| Z29 | 0.13 | 0.41 | 5.71 | 0.94 | 0.32 | 0.85 | 2014.84 | 7.43 | 1932.18 | 8.14 | 1810.50 | 13.42 | 0.89 | 0.43 | 93.70 |
| Z30 | 0.13 | 0.95 | 5.04 | 2.74 | 0.29 | 2.56 | 2013.24 | 17.40 | 1826.77 | 23.18 | 1626.23 | 36.86 | 0.94 | 0.42 | 89.02 |

Table 5 - Summary of LA-ICP-MS data of zircons from sample LS-65 (Floresta Suite).

| Grain spot | Isotopic ratios $^{207}Pb/^{206}Pb$ | ± (1σ) | $^{207}Pb/^{235}U$ | ± (1σ) | $^{206}Pb/^{238}U$ | ± (1σ) | Ages $^{207}Pb/^{206}Pb$ | ± (1σ) | $^{207}Pb/^{235}U$ | ± (1σ) | $^{206}Pb/^{238}U$ | ± (1σ) | Rho | Th/U | Conc. (%) |
|---|---|---|---|---|---|---|---|---|---|---|---|---|---|---|---|
| Z01 | 0.13 | 0.45 | 6.76 | 0.77 | 0.38 | 0.63 | 2039.75 | 8.24 | 2080.37 | 6.84 | 2070.58 | 11.11 | 0.77 | 0.58 | 99.53 |
| Z02 | 0.13 | 0.36 | 6.50 | 0.70 | 0.36 | 0.61 | 2042.20 | 6.55 | 2045.94 | 6.20 | 2000.06 | 10.42 | 0.82 | 0.73 | 97.76 |
| Z03 | 0.13 | 0.44 | 6.43 | 0.71 | 0.36 | 0.55 | 2035.44 | 8.07 | 2036.29 | 6.24 | 1987.78 | 9.48 | 0.72 | 0.80 | 97.62 |
| Z04 | 0.13 | 0.52 | 6.58 | 0.82 | 0.37 | 0.63 | 2043.75 | 9.40 | 2056.50 | 7.20 | 2019.23 | 10.97 | 0.73 | 0.74 | 98.19 |
| Z05 | 0.13 | 0.64 | 6.15 | 0.98 | 0.35 | 0.74 | 2037.65 | 11.73 | 1997.98 | 8.60 | 1912.12 | 12.32 | 0.72 | 0.49 | 95.70 |
| Z06 | 0.13 | 0.59 | 6.23 | 0.84 | 0.35 | 0.60 | 2035.56 | 10.74 | 2008.48 | 7.37 | 1934.05 | 10.04 | 0.66 | 0.56 | 96.29 |
| Z07N | 0.13 | 0.46 | 5.53 | 0.72 | 0.32 | 0.55 | 2003.01 | 8.47 | 1904.85 | 6.19 | 1771.35 | 8.54 | 0.70 | 0.09 | 92.99 |
| Z07B | 0.12 | 0.44 | 4.33 | 1.14 | 0.25 | 1.05 | 1953.94 | 8.06 | 1698.75 | 9.39 | 1461.92 | 13.74 | 0.92 | 0.12 | 86.06 |
| Z08 | 0.13 | 0.61 | 6.11 | 0.94 | 0.34 | 0.71 | 2039.00 | 11.18 | 1992.07 | 8.18 | 1899.68 | 11.64 | 0.72 | 0.49 | 95.36 |
| Z09 | 0.13 | 0.53 | 6.65 | 1.07 | 0.37 | 0.93 | 2043.85 | 9.70 | 2066.66 | 9.43 | 2039.20 | 16.19 | 0.85 | 0.65 | 98.67 |
| Z10 | 0.13 | 0.34 | 6.33 | 0.62 | 0.35 | 0.52 | 2040.58 | 6.10 | 2021.94 | 5.44 | 1955.08 | 8.81 | 0.78 | 0.82 | 96.69 |
| Z11 | 0.13 | 0.37 | 6.32 | 0.78 | 0.35 | 0.69 | 2035.38 | 6.75 | 2020.66 | 6.86 | 1957.59 | 11.63 | 0.86 | 0.58 | 96.88 |
| Z12 | 0.13 | 0.38 | 5.68 | 0.81 | 0.32 | 0.71 | 2009.51 | 6.93 | 1929.02 | 6.96 | 1809.48 | 11.23 | 0.86 | 0.21 | 93.80 |
| Z13 | 0.13 | 0.52 | 6.17 | 0.89 | 0.34 | 0.72 | 2043.24 | 9.49 | 1999.88 | 7.76 | 1910.49 | 11.87 | 0.78 | 0.68 | 95.53 |
| Z14N | 0.13 | 0.39 | 6.44 | 0.75 | 0.36 | 0.64 | 2044.60 | 7.12 | 2037.63 | 6.59 | 1981.54 | 10.90 | 0.82 | 0.63 | 97.25 |
| Z14B | 0.13 | 0.47 | 5.98 | 0.72 | 0.34 | 0.55 | 2024.69 | 8.50 | 1973.45 | 6.26 | 1877.95 | 8.94 | 0.70 | 0.42 | 95.16 |
| Z15N | 0.13 | 0.54 | 6.17 | 0.85 | 0.35 | 0.66 | 2042.17 | 9.90 | 2000.90 | 7.47 | 1913.43 | 10.91 | 0.73 | 0.68 | 95.63 |
| Z15B | 0.13 | 0.64 | 6.43 | 0.91 | 0.36 | 0.64 | 2048.64 | 11.64 | 2036.30 | 7.98 | 1975.06 | 10.94 | 0.66 | 0.74 | 96.99 |
| Z16 | 0.13 | 0.61 | 6.55 | 1.03 | 0.37 | 0.82 | 2025.66 | 11.17 | 2052.55 | 9.05 | 2029.21 | 14.36 | 0.78 | 0.85 | 98.86 |
| Z17 | 0.13 | 0.41 | 6.01 | 0.76 | 0.34 | 0.64 | 2014.36 | 7.40 | 1977.17 | 6.63 | 1894.46 | 10.57 | 0.81 | 0.20 | 95.82 |
| Z18 | 0.13 | 0.31 | 6.00 | 0.62 | 0.34 | 0.53 | 2021.27 | 5.68 | 1976.41 | 5.38 | 1886.63 | 8.73 | 0.81 | 0.25 | 95.46 |
| Z19 | 0.13 | 0.31 | 6.21 | 0.65 | 0.35 | 0.57 | 2030.22 | 5.56 | 2006.26 | 5.69 | 1934.85 | 9.60 | 0.85 | 0.74 | 96.44 |
| Z20 | 0.13 | 0.51 | 6.46 | 0.83 | 0.36 | 0.65 | 2026.95 | 9.36 | 2040.68 | 7.29 | 2004.59 | 11.21 | 0.74 | 0.69 | 98.23 |

| | | | | | | | | | | | | | | | | |
|---|---|---|---|---|---|---|---|---|---|---|---|---|---|---|---|---|
| Z21 | 0.13 | 0.46 | 6.55 | 0.93 | 0.37 | 0.81 | 2034.66 | 8.43 | 2052.59 | 8.19 | 2020.46 | 13.97 | 0.85 | 0.85 | 98.43 |
| Z22 | 0.13 | 0.30 | 6.67 | 0.64 | 0.37 | 0.56 | 2038.61 | 5.54 | 2068.13 | 5.62 | 2047.29 | 9.80 | 0.84 | 0.74 | 98.99 |
| Z23 | 0.13 | 0.52 | 6.49 | 0.93 | 0.37 | 0.78 | 2017.92 | 9.40 | 2044.98 | 8.21 | 2021.86 | 13.49 | 0.81 | 0.61 | 98.87 |
| Z24 | 0.13 | 0.45 | 6.43 | 0.82 | 0.36 | 0.68 | 2024.19 | 8.18 | 2036.65 | 7.18 | 1999.40 | 11.74 | 0.81 | 0.65 | 98.17 |
| Z25 | 0.13 | 0.66 | 6.00 | 1.09 | 0.34 | 0.88 | 2026.49 | 11.94 | 1975.45 | 9.51 | 1880.03 | 14.27 | 0.78 | 0.45 | 95.17 |
| Z26 | 0.12 | 0.46 | 5.32 | 0.86 | 0.31 | 0.72 | 1971.43 | 8.42 | 1872.71 | 7.33 | 1741.01 | 11.04 | 0.82 | 0.73 | 92.97 |
| Z27 | 0.13 | 0.63 | 6.24 | 0.96 | 0.35 | 0.72 | 2045.41 | 11.46 | 2009.74 | 8.36 | 1927.16 | 11.96 | 0.72 | 0.64 | 95.89 |

Table 6 - Summary of LA-ICP-MS data of zircons from sample LS-60 (Floresta Suite).

| Sample | Unit | Sm (ppm) | Nd (ppm) | $^{143}Nd/^{144}Nd$ (±2SE) | εNd (0) | εNd (t) | U-Pb age (Ga) | $T_{DM}$ (Ga) |
|---|---|---|---|---|---|---|---|---|
| FL105 | R.L.S. | 2.28 | 17.07 | 0.510515 (±17) | -41.41 | -2,001 | 2.648 | 2.90 |
| FL53 | R.L.S. | 4.50 | 33.53 | 0.510637 (±20) | -39.04 | 0,361 | 2.648 | 2.76 |
| FL58 | R.L.S. | 2.92 | 23.14 | 0.510522 (±14) | -41.28 | -0,251 | 2.648 | 2.79 |
| FL46a | R.L.S. | 2.37 | 19.88 | 0.510477 (±19) | -42.15 | 0,238 | 2.648 | 2.76 |
| FL56 | R.L.S. | 1.87 | 16.01 | 0.510430 (±12) | -43.08 | -0,205 | 2.648 | 2.78 |
| FL57 | R.L.S. | 2.35 | 17.26 | 0.510587 (±09) | -40.01 | -1,101 | 2.648 | 2.85 |
| FL54B | R.L.S. | 2.01 | 12.15 | 0.510864 (±05) | -34.62 | -1,802 | 2.648 | 2.93 |
| FL 70 | F.S. | 1.56 | 12.06 | 0.511049 (±18) | -31.00 | +0.94 | 2.098 | 2.23 |
| FL67 | F.S. | 7.85 | 35.43 | 0.511818 (±18) | -15.99 | +0.91 | 2.098 | 2.33 |
| Fl 106a | F.S. | 4.09 | 18.53 | 0.511547 (±17) | -21.28 | -4.33 | 2.098 | 2.86 |
| FL 95b | F..S. | 1.93 | 9.162 | 0.511897 (±03) | -14.45 | +4.24 | 2.098 | 2.01 |
| FL 65 | F.S. | 3.74 | 18.15 | 0.511590 (±08) | -20.44 | -0.99 | 2.098 | 2.48 |
| FL 73 | F.S. | 4.88 | 25.17 | 0.511588 (±15) | -20.48 | +0.92 | 2.098 | 2.29 |
| FL 104a | F.S. | 1.33 | 10.27 | 0.516031 (±25) | -39.15 | -7.36 | 2.098 | 2.72 |
| Fl 66 | F.S. | 11.83 | 69.88 | 0.510722 (±19) | -37.38 | -12.03 | 2.098 | 3.19 |
| Fl 59 | F.S. | 2.69 | 18.86 | 0.510594 (±16) | -39.87 | -10.17 | 2.098 | 2.93 |
| Fl 40 | F.S. | 2.84 | 17.04 | 0.511191 (±08) | -28.23 | -2.42 | 2.098 | 2.49 |

| | | | | | | | | |
|---|---|---|---|---|---|---|---|---|
| Fl 102 | F.S. | 10.04 | 80.02 | 0.510671 (±19) | -38.37 | -5.85 | 2.098 | 2.36 |
| Fl 32a | F.S. | 10.05 | 76.46 | 0.510751 (±04) | -36.81 | -5.25 | 2.098 | 2.60 |
| Fl 88 | F.S. | 0.54 | 3.018 | 0.511660 (±10) | -19.08 | +4.47 | 2.098 | 2.01 |
| Fl 69 | F.S. | 3.48 | 17.72 | 0.511553 (±13) | -21.17 | -0.17 | 2.098 | 2.38 |
| Fl 60 | F.S. | 4.76 | 26.70 | 0.511388 (±05) | -24.38 | -0.45 | 2.098 | 2.37 |
| Fl 68 | F.S. | 2.72 | 19.42 | 0.511112 (±18) | -29.77 | +0.45 | 2.098 | 2.27 |
| Fl 62 | F.S. | 8.96 | 47.45 | 0.511552 (±14) | -21.18 | +1.05 | 2.098 | 2.27 |

Table 7 - Summary of Nd isotope data for the metaplutonic rocks of Riacho das Lajes (R.L.S.) and Floresta Suites (F.S.).

Highlights

> First record of Archean Continental Crust in Central Subprovince of the Borborema Province

> Geochemical and isotopic data reveals a complex accretionary history for the Alto Moxotó Terrane

> Our data provide evidence for new Neoarchean crustal growth and Paleoproterozoic reworking in central Western Gondwana